DOE/JPL/954901-79/6

DEVELOPMENT AND EVALUATION OF DIE MATERIALS FOR USE IN THE GROWTH OF SILICON RIBBONS BY THE INVERTED RIBBON GROWTH PROCESS—TASK II—LSA PROJECT

Final Report for October 1, 1977—March 31, 1979

By
M. T. Duffy
S. Berkman
G. W. Cullen
R. V. D'Aiello
H. I. Moss

December 1979

Work Performed Under Contract No. NAS-7-100-954901

RCA Laboratories
Princeton, New Jersey

U.S. Department of Energy

Solar Energy

DISCLAIMER

DISCLAIMER

Available from the National Technical Information Service, U. S. Department of Commerce, Springfield, Virginia 22161.

Price: Paper Copy $7.00
Microfiche $3.50

DOE/JPL/954901-79/6
Distribution Category UC-63b

DRL Line Item No. 10

DEVELOPMENT AND EVALUATION OF DIE MATERIALS FOR USE IN THE GROWTH OF SILICON RIBBONS BY THE INVERTED RIBBON GROWTH PROCESS — TASK II — LSA PROJECT

M. T. Duffy, S. Berkman, G. W. Cullen,
R. V. D'Aiello, and H. I. Moss

RCA Laboratories
Princeton, New Jersey 08540

FINAL REPORT

December 1979

This work was performed for the Jet Propulsion Laboratory, California Institute of Technology, under NASA Contract NAS7-100 for the Department of Energy.

The JPL Low-Cost Solar Array Project is funded by DOE and forms part of the DOE Photovoltaic Conversion Program to initiate a major effort toward the development of low-cost solar arrays.

Prepared Under Contract No. 954901 For
JET PROPULSION LABORATORY
CALIFORNIA INSTITUTE OF TECHNOLOGY
Pasadena, California 91103

THIS PAGE

WAS INTENTIONALLY

LEFT BLANK

PREFACE

This Final Report, prepared by RCA Laboratories, Princeton, NJ 08540, describes work performed for the period October 1, 1977 through March 31, 1979, under Contract No. 954901 in the Materials and Processing Research Laboratory, D. Richman, Director. G. W. Cullen is the Group Head and the Project Supervisor. M. T. Duffy is the Project Scientist.

Others who participated in the research and writing of this report are

W. H. Bleacher J. F. Corboy R. A. Soltis H. E. Temple	- Technical assistance
R. J. Paff	- X-ray analysis
H. H. Whitaker	- Emission spectroscopic analysis
P. J. Zanzucchi	- Infrared measurements
K. M. Kim* S. H. McFarlane	Crystallographic analysis of silicon ribbon (Appendix II)

Technical discussions with T. P. O'Donnell and M. Leipold of Jet Propulsion Laboratory have been very helpful.

The RCA Report No. is PRRL-79-CR-34.

*Present address is IBM, Data Systems Div., E. Fishkill Laboratory, Hopewell Junction, NJ.

TABLE OF CONTENTS

LIST OF ILLUSTRATIONS

LIST OF TABLES

SECTION I

SUMMARY

Amorphous CVD layers of silicon nitride and silicon oxynitride are prepared by chemical vapor deposition (CVD). The CVD layers are converted to α- and β-Si_3N_4 in contact with molten silicon. Silicon nitride layers are converted initially to α-Si_3N_4 with a low β-Si_3N_4 content. The α phase is then slowly converted to the β phase accompanied by simultaneous decomposition. By contrast, silicon oxynitride (SiO_xN_y) layers are converted predominantly to β-Si_3N_4 with a low α-Si_3N_4 content. In this process, oxygen is evolved, and there is no evidence for the existence of an oxynitride phase in the resulting layers. The analysis also indicates that β-Si_3N_4 is much more resistant to chemical attack by molten silicon than α-Si_3N_4. Consequently, CVD silicon oxynitride provides a useful means of obtaining relatively pure and inert β-Si_3N_4 as a substrate coating for prolonged exposure to molten silicon, while CVD silicon nitride coatings are useful for shorter exposure times.

Crystallographic analysis of silicon ribbon test specimens, grown from CVD-coated vitreous carbon dies, indicates that silicon carbide inclusions are not present in the ribbon samples. The results of infrared analysis also show that the carbon content of the silicon ribbons is below detection level and lower than in the Czochralski seed material.

SECTION II

INTRODUCTION

There has been no material found to date which is completely inert to the solvent nature of molten silicon. The search for viable cost-effective crucible and die materials for the production of solar-cell-grade silicon continues with increasing emphasis on purity and inertness. Since all contact materials currently employed react with molten silicon to some extent, it is important that these materials be as pure as possible so as not to degrade solar-cell efficiency. A discussion of materials properties and considerations has been presented elsewhere[1,2].

The objective of this program was to develop and evaluate die materials for use in the growth of silicon ribbons by the inverted ribbon growth process (IRG) [3] and for other applications. The major emphasis was on developing CVD coatings of Si_3N_4 and SiO_xN_y on suitable die materials and studying the stability and interaction of these layers with molten silicon. The dies were tested in silicon ribbon growth experiments and evaluated analytically. The ribbons were characterized electrically, crystallographically, and in solar cells. Both CVD-coated dies and crucibles were fabricated, and deposition parameters were adjusted, where possible, to favor reduced cost. The performance goals required that dies be dimensionally stable to within 0.5 mil over a 24-h period at ~1425°C, and that the dies should not excessively contaminate silicon processed through them.

1. T. O'Donnell, M. Leipold, and M. Hagan, "Compatibility Studies of Various Refractory Materials in Contact with Molten Silicon," DOE/JPL-1012-77/6, March 1978.
2. M. H. Leipold, T. P. O'Donnell, and M. A. Hagan, J. Cryst. Growth., to be published.
3. K. M. Kim, S. Berkman, M. T. Duffy, A. E. Bell, H. E. Temple, and G. W. Cullen, "Silicon Sheet Growth by the Inverted Stepanov Technique," Final Report, prepared for Jet Propulsion Laboratory, DOE/JPL954465-77/2, June 1977.

SECTION III

EXPERIMENTAL

Silicon nitride layers were deposited on various substrates by the reaction between silane, SiH_4, and ammonia, NH_3. The carrier gas was either hydrogen or nitrogen, and the deposition temperature was 1000°C. The NH_3:SiH_4 ratio was initially 100:1 and subsequently 33:1, although lower ratios were also investigated. Silicon oxynitride layers were prepared in a similar fashion except that nitrous oxide, N_2O, was introduced as the oxygen-containing reagent. The ratio of NH_3:N_2O was 10:1 in all cases. Deposition was performed in a barrel reactor of the type described previously[4-6].

Substrate materials were usually obtained commercially. Hot-pressed Si_3N_4 was also prepared in-house from commercially available powders.

Materials were evaluated in silicon sessile drop experiments and, in the case of CVD materials, by silicon ribbon growth from coated dies. The sessile drop experiments were performed by maintaining a molten silicon droplet at about 1450°C on the sample surface in ultrapure helium. The furnace was heated by a tungsten mesh element and had water-cooled stainless steel walls. After the tests, samples were sectioned through the solidified silicon and polished. Some samples were also etched slightly to provide greater contrast for microscopic examination of the interface region between silicon and substrate. The sections were examined microscopically for evidence of reaction or new phases. Resistivity measurements were made on the sectioned faces of the silicon droplets as a guide to contamination effects. These measurements were made at several positions on each sample to minimize the influence of cracks and grain structure on the measurements.

The die configuraton and assembly used in the growth of silicon ribbon test specimens have been described previously[3]. It consisted of a V-shaped die with a capillary at the bottom from which the ribbon specimens were pulled.

4. G. W. Cullen, J. F. Corboy, and R. T. Smith, J. Cryst. Growth 31, 274 (1975).
5. G. W. Cullen, Heteroepitaxial Semiconductors for Electronic Devices (Springer-Verlag, New York, 1978), p. 60.
6. S. Berkman, V. S. Ban, and N. Goldsmith, Heteroepitaxial Semiconductors for Electronic Devices (Springer-Verlag, New York, 1978), p. 264.

Electrical testing was performed by solar-cell evaluation, minority-carrier lifetime measurements, and by four-point-probe resistivity measurements.

SECTION IV

RESULTS AND DISCUSSION

A. Sessile Drop Experiments with Sintered and Hot-Pressed Materials

Various refractory materials were evaluated in silicon sessile drop experiments to ascertain the most suitable candidates for further study as die materials or substrates for CVD layers. The refractories included carbides, nitrides, and oxides and were tested in contact with molten silicon at 1440°C in ultrapure He for 30 min. The properties of greatest interest were purity and inertness. A summary of our observations is presented in Table 1. Section micrographs are provided for a few cases in Appendix I. Approximate resistivity values are also given in Table 1 for those cases where the molten silicon was not totally absorbed by the substrate. The resistivity of the silicon used was nominally about 1000 Ω-cm. As expected, none of the materials examined were completely inert to molten silicon or free from contamination effects. The materials which exhibited the most useful properties were hot-pressed Si_3N_4, reaction-sintered Si_3N_4, sintered ZrO_2, and vitreous carbon. Boron-containing materials such as BN and LaB_6 reacted only slightly with molten silicon, but proved to be sources of unacceptable amounts of electrically active boron. It should be kept in mind that a carrier concentration of $\sim 2 \times 10^{16}$ atoms/cm^3 is equivalent to 1 ppm in silicon. It is important to note in these experiments that such factors as purity, density, stoichiometry, crystallinity, and phases present are important factors in determining the usefulness of a given material. Since these properties are frequently not well defined, there is reason for caution in making a definitive statement about the usefulness of a given material.

B. SESSILE DROP EXPERIMENTS WITH CVD MATERIALS

The results of sessile drop experiments conducted on CVD Si_3N_4 and CVD SiO_xN_y are also presented in Table 1 for comparison purposes. It can be seen that contamination of the silicon, as indicated by resistivity, is reduced by the presence of the CVD coatings on the same substrates tested above, even when the CVD layer was cracked, as in the case of Si_3N_4 on vitreous carbon. In addition, CVD SiO_xN_y coatings are capable of withstanding prolonged exposure to molten silicon as shown by the last entry in Table 1. A section

TABLE 1. DATA FROM SESSILE DROP TESTS

Material	Si Resistivity Ω-cm	Comments
TiC (HP*)	--	porous, Si absorbed, reacted interfacial layer
ZrC (HP)	--	porous, Si absorbed
HfC (HP)	--	porous, Si absorbed
TaC (HP)	--	reacted with Si completely
TiN (HP)	--	deep penetration of Si in TiN and formation of another phase in Si
ZrN (HP)	too low to measure	deep penetration of Si with formation of reaction zone in ZrN
AlN (HP)	too low to measure	deep penetration of Si with possible formation of another phase along the boundary region of Si
AlN + 5% SiC (HP)	too low to measure	particulate erosion with precipitation of a crystalline phase in Si, possibly SiC
Si_3N_4 (RS)†	0.2	particulate erosion with formation of crystallites in Si at interface
Si_3N_4 (HP) (99.2% theoretical density)	1	after 4 h at 1450°C, no apparent reaction
TiO_2 (conventionally sintered)	too low to measure	extensive reaction
ZrO_2 (conventionally sintered)	0.2	penetration of Si with probable formation of another phase in ZrO_2
HfO_2 (single crystal)	too low to measure	formation of another phase in Si along boundary with HfO_2
ThO_2 (HP)	too low to measure	slight penetration of Si and formation of eutectic phase in Si
LaB_6 (HP)	too low to measure	no apparent reaction
$MoSi_2$ (HP)	--	Si absorbed
Mullite (85% mullite + 15% glass)	~0.05	after 1 h at 1450°C, interfacial reaction
CVD Si_3N_4/(85% mullite + 15% glass)	~0.3	after 1 h at 1450°C, CVD layer cracked, β-Si_3N_4 crystallites at Si/layer interface
Vitreous carbon	0.8	interfacial phase formed
CVD Si_3N_4 on vitreous carbon	8.4	CVD layer cracked, Si penetration at cracks
CVD Si_3N_4/RS† Si_3N_4	18-34	after 4 h at 1440°C
CVD SiO_xN_y/RS Si_3N_4	2.8-8	after 4 h at 1440°C
CVD SiO_xN_y/RS Si_3N_4	0.2-0.8	after 22 h at 1440°C

Note: The silicon used in these tests was "Hyper-Pure" material (from Dow Corning Corp.) with $\rho > 1000$ Ω-cm. The duration of the sessile drop tests was 30 min in all cases except for Si_3N_4 (HP), mullite, and the last three samples shown in the table. The resistivities shown here are approximate values.

*HP = hot-pressed.

†RS = reaction sintered.

view of this sample is shown in Fig. 1. Preliminary studies on these layers have been described previously[3]. Both CVD Si_3N_4 and CVD SiO_xN_y act as useful barriers to impurity diffusion from the substrate into the silicon melt. The composition of the SiO_xN_y layers used here is not known at this time, but the atomic ratio of oxygen to nitrogen is expected to be about one in amorphous layers deposited at 1000°C. Subsequent heating to the melting point of silicon, however, causes crystallization and change in composition. This will be discussed later. The initial composition is not critical.

The silicon nitride and oxynitride layers discussed above were prepared by the reaction between ammonia and silane using the ratio NH_3:SiH_4 = 100:1. It has been generally recognized in the semiconductor literature that amorphous Si_3N_4 films prepared with a ratio less than the above value are silicon-rich in composition. The cost of ammonia (minimum purity 99.999%) using this ratio, represents 90% of the estimated cost of depositing these layers in a production facility. Consequently, a reduction in this ratio could mean a substantial reduction in cost, provided the rate of erosion of the CVD layers in contact with molten silicon is not seriously affected. We have also prepared CVD Si_3N_4 layers on vitreous carbon at the following ammonia to silane ratios, 33:1, 20:1, 10:1, and 5:1, and performed a preliminary evaluation of the layers in sessile drop experiments. No noticeable change in erosion rate was observed at a ratio of 33:1. Consequently, this latter ratio has been used in subsequent preparation of CVD coatings. It appears from the limited number of experiments performed that it may be possible to use coatings deposited at even lower ratios without appreciably altering the useful life of the layers. At a ratio of NH_3:SiH_4 = 5:1 the wetting characteristics of the CVD Si_3N_4 layers changed to a lower contact angle, and surface wetting occurred more readily.

C. THERMAL STABILITY OF CVD LAYERS

1. CVD Si_3N_4

As-deposited Si_3N_4 layers were amorphous in character. Figure 2 shows the infrared transmission spectrum corresponding to a 1-μm-thick CVD layer on a silicon substrate both before and after heat treatment. The spectrum of the as-deposited material displays typical amorphous character, while heat treatment in He at 1400°C for 1 h results in a spectrum which displays the structure of crystalline material. A point of interest here is that

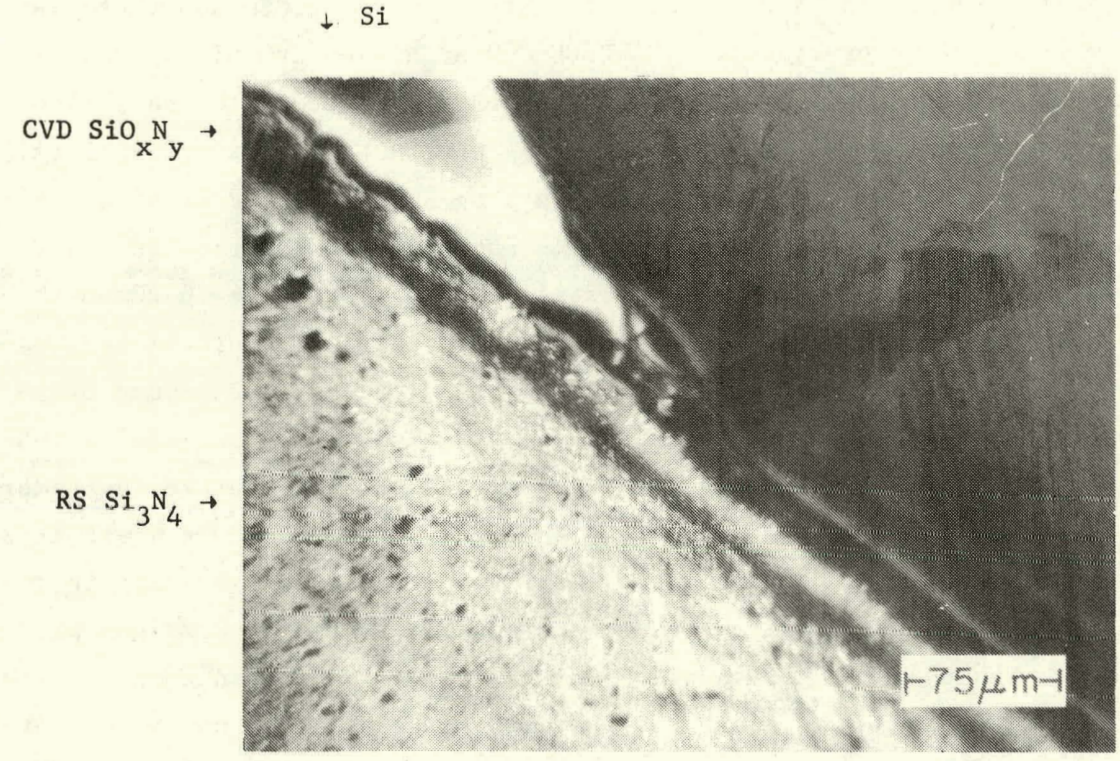

(a)

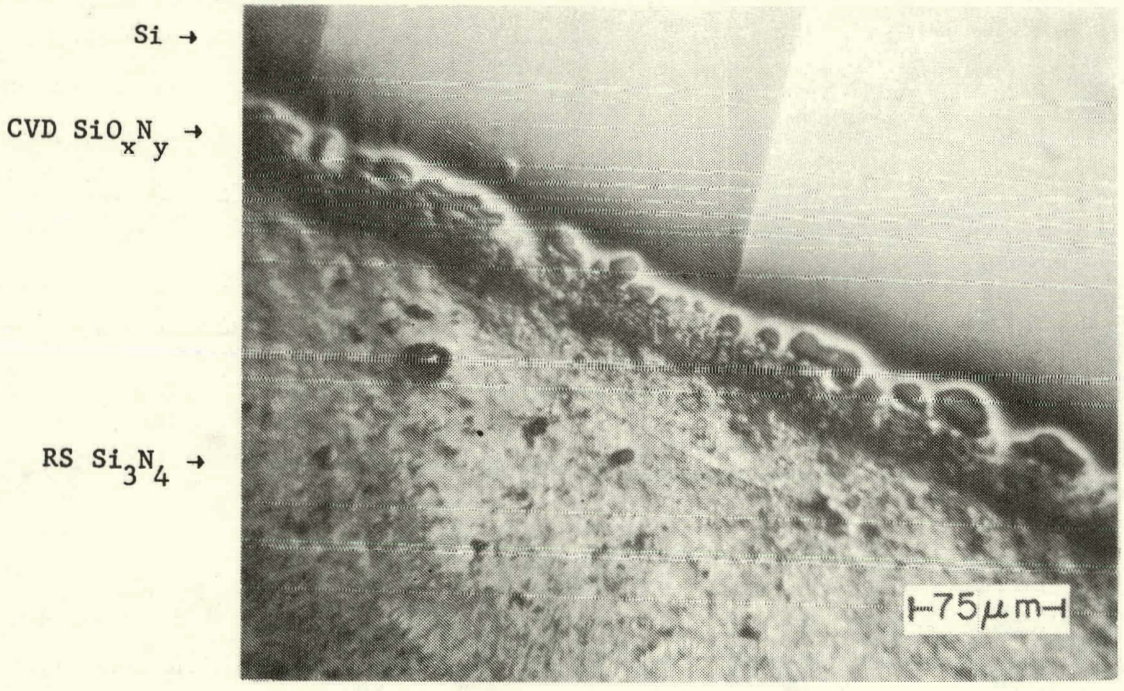

(b)

Figure 1. Photograph of a sectioned Si/CVD SiO_xN_y/RS Si_3N_4 sample showing film continuity; (a) near edge of silicon droplet, and (b) under silicon droplet after 22 hours at 1440°C.

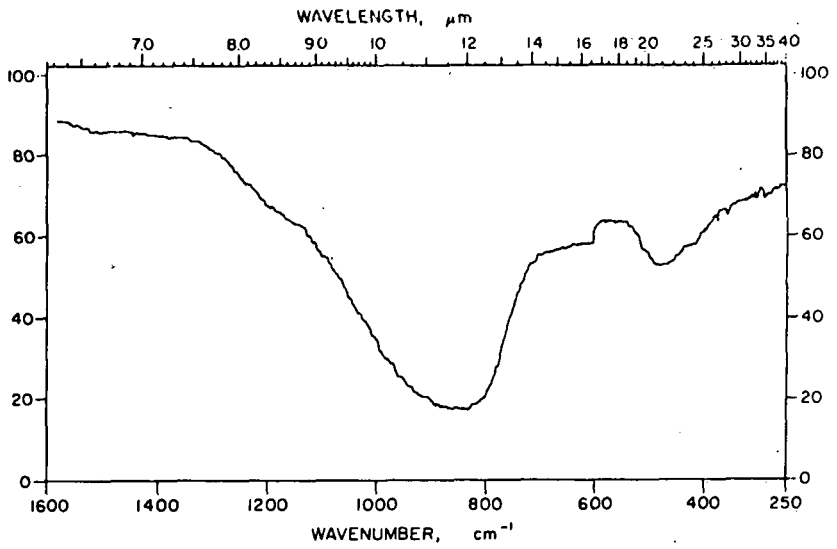

(a)

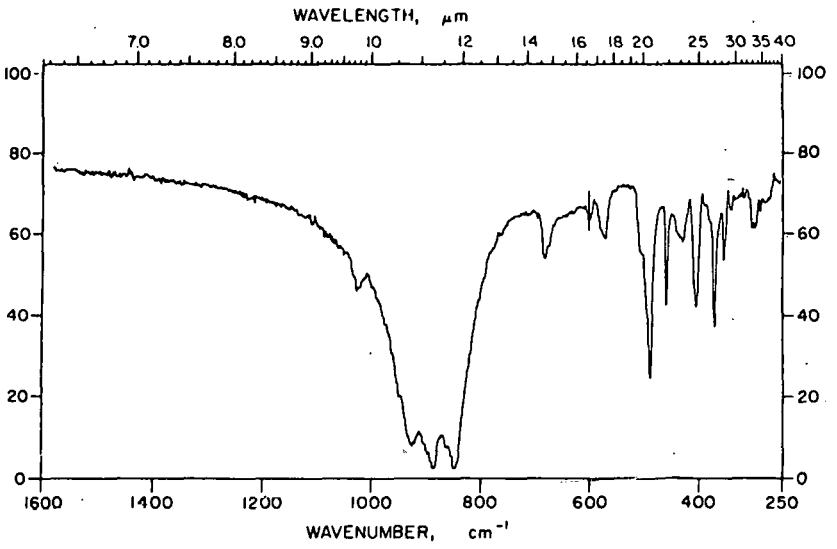

(b)

Figure 2. Transmission infrared spectra of CVD-Si_3N_4 corresponding to: (a) amorphous as-prepared sample and, (b) sample after crystallization at 1400°C in He for 1 h.

there is no evidence in these spectra for the existence of Si-H or N-H bonding in these layers[7]. The deposition temperature was chosen so as to avoid these effects. The estimated phase content of the layer after heat treatment, as determined by x-ray diffraction, was about 90% α-Si_3N_4 and 10% β-Si_3N_4.

The composition of a relatively thick (~9 mil) CVD Si_3N_4 layer after heating at 1500°C in He for prolonged periods is shown in Table 2. This sample, prior to heat treatment, was removed from the susceptor used in the deposition system. There is an apparent transition from the α phase to the β phase accompanied by decomposition as revealed by the increase in free silicon content as a result of prolonged heating. It is interesting to note that there is a relative increase in the β-phase content despite the fact that decomposition is also taking place. This indicates that the β phase is the more stable form under these conditions. Microscopic examination of a polished section of the same layer, after heating for 34 h at 1500°C in He, showed that the sample had a porous texture on both surfaces but appeared to be quite dense in the center region of the sample. X-ray diffraction (powder) patterns were obtained on specimens from the three regions - both faces of the sample and central region. The results are given in Table 3. A portion of the same sample was etched in a mixture of HNO_3 + HF, to selectively remove excess silicon which might be accessible to the etchant, and x-ray diffraction patterns again obtained on the corresponding three regions. The results are also presented in Table 3. The designation "front surface" in Table 3 refers to the surface which was exposed to the He ambient during heat treatment. The back surface corresponds to that which was in contact with a horizontal susceptor during heat treatment.

The results presented in Table 3 show variation in phase content between the different regions of the layer. There is a decrease in the percentage of α-phase content in going from the front surface to the back surface, and a simultaneous increase in the β-phase content. All of the sample was sufficiently porous to allow the etchant to penetrate the layer. However, microscopic examination showed that the central region was still much more dense after etching than the surface regions. The variation in phase content

7. H. J. Stein and H. A. R. Wegener, J. Electrochem. Soc. 124, 908 (1977).

TABLE 2. PHASES PRESENT IN CVD Si_3N_4 LAYER AS A FUNCTION OF TIME OF HEATING IN He AT 1500°C

Approximate Content			Time at 1500°C
α-Si_3N_4	β-Si_3N_4	Si	(hours)
80%	20%	-	0.5
75%	20%	5%	3
75%	20%	5%	5.5
15%	40%	45%	30

TABLE 3. PHASES PRESENT IN CVD Si_3N_4 LAYER AFTER HEATING AT 1500°C FOR 34 HOURS IN HE

	Approximate Content (before etching)			Approximate Content (after etching)		
	α-Si_3N_4	β-Si_3N_4	Si	α-Si_3N_4	β-Si_3N_4	Si
Front Surface	45%	15%	40%	70%	30%	~1%
Central Region	25%	45%	30%	33%	66%	~1%
Back Surface	14%	43%	43%	25%	75%	~1%

from the front surface to the back surface is probably due to a corresponding thermal gradient in the sample, and the decomposition rate is higher at exposed surfaces.

The rates of phase-conversion and decomposition at a given temperature are higher when CVD Si_3N_4 is exposed to molten silicon. If silicon is selectively etched from the CVD layer after contact with the silicon melt, needle-like crystallites of β-Si_3N_4 (identified by x-ray analysis) are observed on the sample surface. In silicon sessile drop experiments, these crystallites are found at the silicon/CVD-layer interface. In silicon ribbon growth experiments, the crystallites nucleate on the cooler parts of the die inside the silicon liquid and grow into the melt, apparently by a transport process from the hotter walls of the system. Simultaneously, the layers in contact with the melt undergo conversion to α- and β-Si_3N_4. The rates of these changes decrease as the β-phase content of the layers increases.

These observations indicate that β-Si_3N_4 is more stable than α-Si_3N_4 under conditions likely to be encountered in silicon ribbon growth. Consequently, some attempts were made to convert the CVD Si_3N_4 layers to β-Si_3N_4 prior to contact with molten silicon. This requires information on the rate of conversion as related to temperature and ambient. The data in Tables 2 and 3 show that conversion is slow at 1500°C. To accelerate the conversion from the α to the β phase, portions of the same layer, used in the experiments corresponding to Tables 2 and 3 above, were heated at 1600°C in N_2 for periods ranging from 1/4 h to a total of 4-1/4 h. The purpose of the N_2 ambient was to suppress decomposition. As before, each sample was analyzed with respect to front surface, central region, and back surface. The results showed little difference in the β-Si_3N_4 content of these three regions for all of the samples and little dependence on time in the range 1/4 to 4-1/4 h. In all cases the α:β ratio was approximately 2, and excess silicon was scarcely detectable in any sample (~1%). Thus, nitrogen suppresses decomposition, but conversion from the α to β phase is still slow, apparently much slower than when in contact with the silicon melt for a given temperature. Nevertheless, an increase in β-phase content can have a significant effect on the durability of these layers in contact with the silicon melt. Attempts to increase the β-phase content of the layers by high-temperature deposition were unsuccessful; α-Si_3N_4 was obtained.

2. CVD SiO_xN_y

The results of preliminary sessile drop experiments indicated that CVD SiO_xN_y layers are more inert to molten silicon than CVD Si_3N_4 layers. The conversion of these layers at high temperature in N_2 was also studied. Some results of x-ray diffraction analysis of these layers on graphite, hot-pressed Si_3N_4, and reaction-sintered Si_3N_4 substrates are presented in Table 4. As shown, conversion to β-Si_3N_4 is much faster than in the case of CVD Si_3N_4 layers. It is interesting to note that there was no evidence of an oxynitride, Si_2ON_2, crystalline phase[8,9] in the heat-treated samples, and excess silicon was not detected. There is, however, a tendency for these layers to flake or crumble when treated in this way. For this reason, conversion in molten silicon is preferable as described below.

8. M. E. Washburn, Ceramic Bulletin 46, 667 (1967).
9. K. H. Jack, J. Mater. Sci. 11, 1135 (1976).

TABLE 4. DEPOSIT PHASE CONTENT AFTER HEAT TREATMENT OF SiO_xN_y SAMPLES

Sample	Treatment	Approximate Content α-Si_3N_4	β-Si_3N_4
CVD SiO_xN_y/graphite	1 h in N_2 at ~1600°C	25%	75%
CVD SiO_xN_y/HP-Si_3N_4	2 h in N_2 at ~1600°C	< 5%	> 95%
CVD SiO_xN_y/RS-Si_3N_4	1 h in N_2 at ~1600°C, 4 h in contact with Si at 1450°C in He	5%	95%

CVD SiO_xN_y layers were also used in silicon sessile drop experiments. Samples were sectioned, examined microscopically, and analyzed for phase content after the selective removal of silicon by etching. The approximate phase content of two such layers after heat treatment in He at 1450°C for 4 h and 20 h, respectively, is shown in Table 5. The data indicate that the layers are converted predominantly to β-Si_3N_4. Longer periods of time in contact with molten silicon favor increased β-phase content, and the rate of conversion to this phase is faster in the presence of molten silicon. The oxynitride layers are converted, predominantly, to β-Si_3N_4 with evolution of oxygen. There is little perceptible change in initial thickness over prolonged periods of time under the above conditions (~40 h of testing). The relative rates of transformation of CVD Si_3N_4 and CVD SiO_xN_y to β-Si_3N_4 make CVD SiO_xN_y layers much more attractive as the starting material. This also explains why oxynitride layers appeared more inert to molten silicon than Si_3N_4 layers in our initial experiments.

Figure 3 shows a section view of a Si/SiO_xN_y/RS-Si_3N_4 composite (from Table 5) which had been heated at 1450°C in He for 4 h. This micrograph was taken at a position adjacent to the silicon sessile drop. A thin film of silicon had spread over the layer surface and appears to have penetrated cracks in the layer [see Fig. 3(a)]. However, when the sample was etched to selectively remove silicon, those features which appeared to be cracks were found to contain a material different in morphology from adjacent portions of the layer as shown in Fig. 3(b). From subsequent x-ray analysis, it is likely that the material in the cracks is β-Si_3N_4, formed by a transport process.

TABLE 5. DEPOSIT PHASE CONTENT AFTER SESSILE DROP TESTS ON SiO_xN_y SAMPLES

Sample	Approximate Content α-Si_3N_4	β-Si_3N_4	Treatment
*Si/SiO_xN_y/RS-Si_3N_4	28%	72%	4 h in He at 1450°C (etched)
†Si/SiO_xN_y/RS-Si_3N_4	22%	78%	4 h in He at 1450°C (etched)
†Si/SiO_xN_y/RS-Si_3N_4	10%	90%	20 h in He at 1450°C (etched)

*region external to silicon droplet

†region under silicon droplet

Figure 4 shows a surface topograph and enlarged section view of the same sample. The surface micrograph displays the presence of a meshlike pattern extended across the surface (as distinct from the "orange-peel" effect of the CVD layer). The transported material is contained in this pattern. The section view in Fig. 4 shows the intersection of one of these regions with the cut face of the sample. A section view corresponding to a cut through the silicon sessile drop on the same sample is shown in Fig. 5. At the interface between the CVD layer and the silicon droplet, needle-like β-Si_3N_4 vertical growth features are apparent. The layer under the silicon droplet also displays a different morphology from that at the bottom portion of the layer. The depth of the transformation to mainly β-Si_3N_4 in the CVD layer is a function of the time of exposure to molten silicon. When the exposure time was increased to 20 h in the case of a second sample (see Table 5), the transformation occurred throughout the depth of the layer. A surface topograph and section view of this sample are presented in Fig. 6. The surface texture is quite different from that shown in Fig. 4(a) because of the longer period of time in contact with molten silicon in the case of this sample. The layer apparently consists of relatively large transparent crystallites as shown in Fig. 6(b). In this case, the CVD layer is approximately 90% β-Si_3N_4 after contact with molten silicon for 20 h. The remaining 10% by volume is α-Si_3N_4, without evidence of an oxynitride, Si_2ON_2, crystalline phase. As indicated in Fig. 6(b), the layer has separated from the substrate.

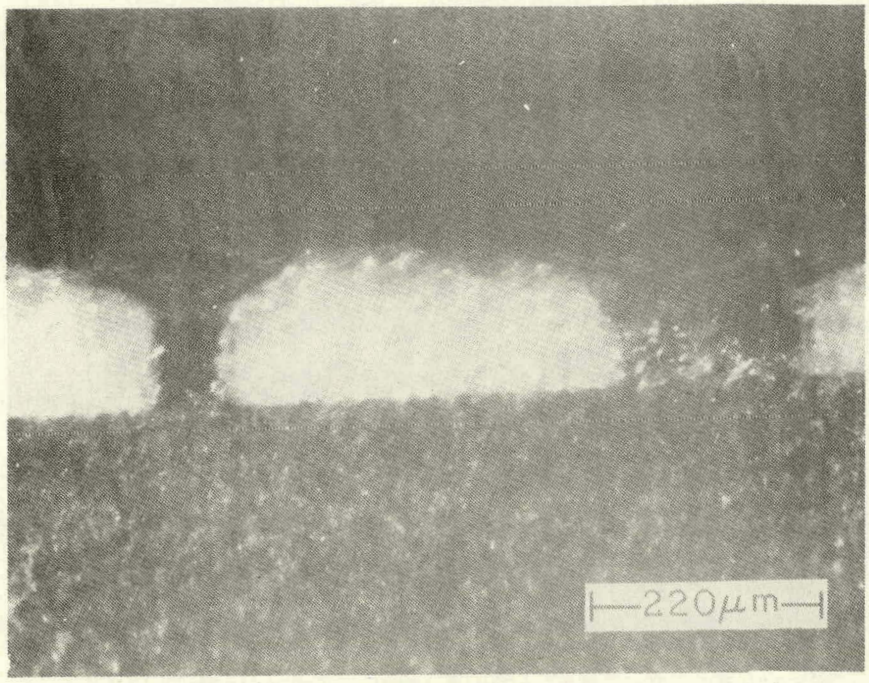

(a)

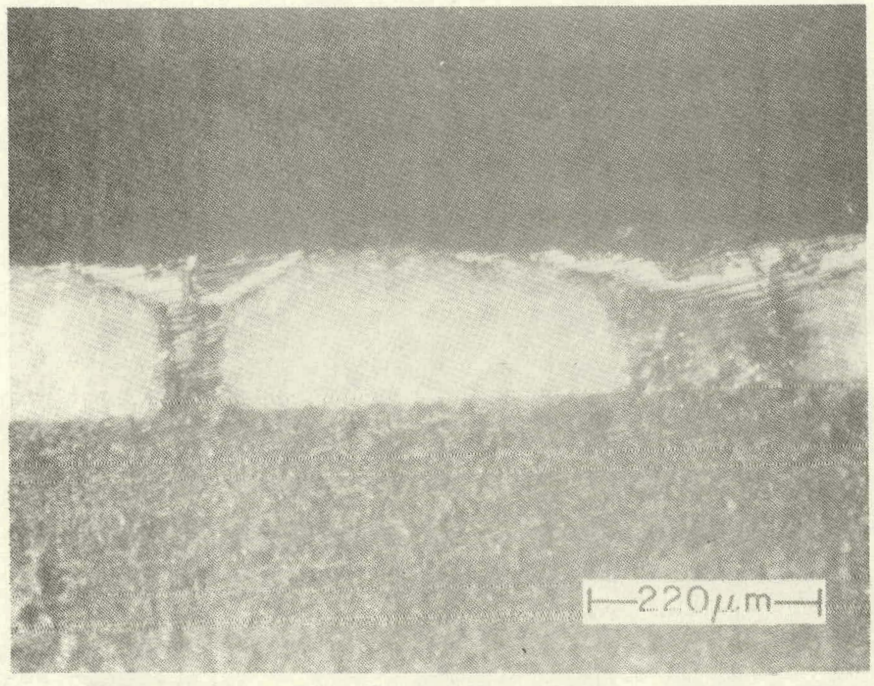

(b)

Figure 3. Section view of $Si/SiO_xN_y/RS\text{-}Si_3N_4$ after 4 h at 1450°C in He; (a) region adjacent to Si droplet before etching, (b) after etching to remove Si.

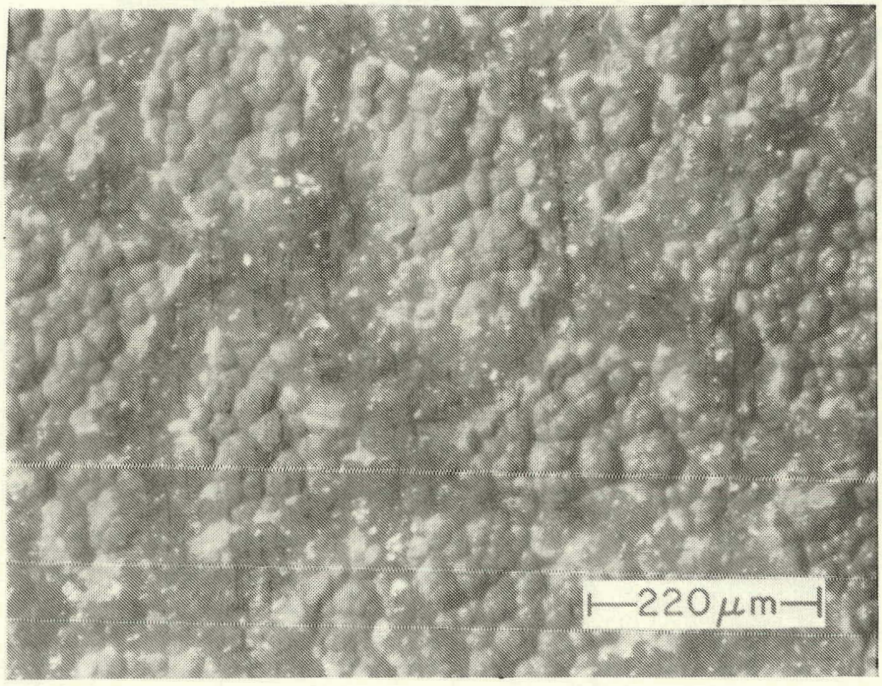

(a)

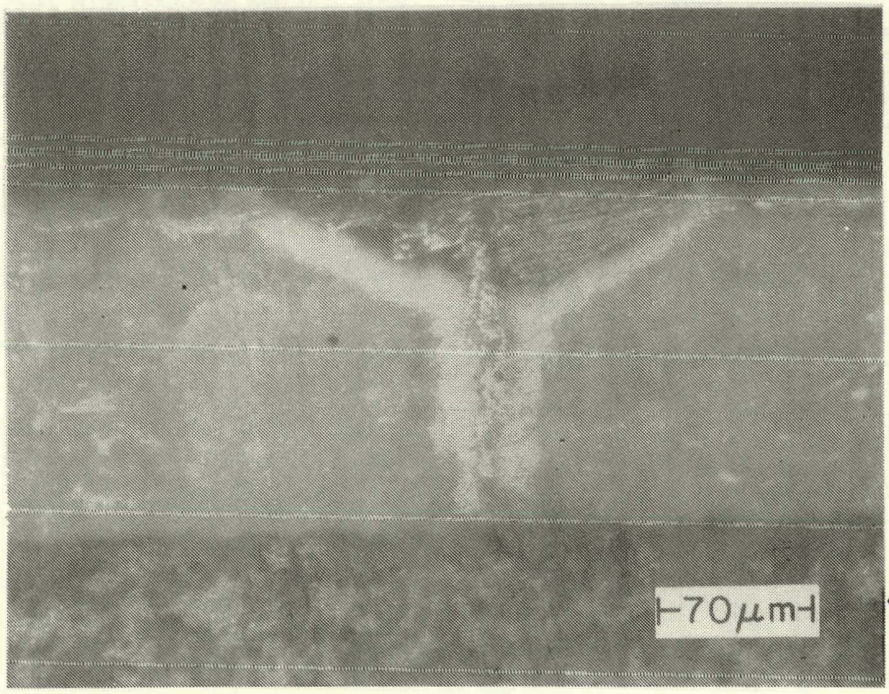

(b)

Figure 4. Surface and section views of etched sample from Fig. 3; (a) showing surface pattern, (b) showing intersection of pattern with plane of cut.

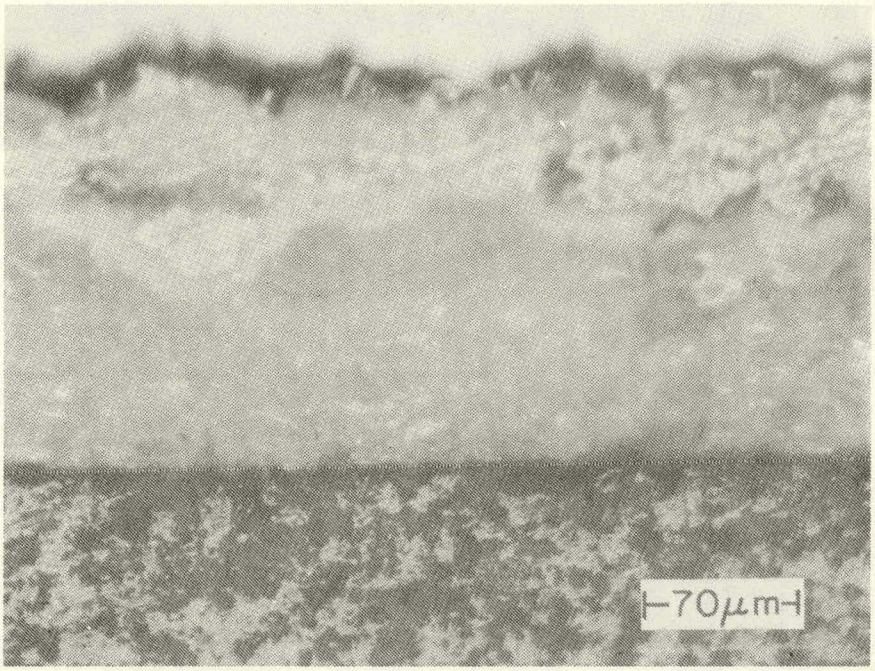

Figure 5. Section view of sample from Fig. 3 under Si droplet.

This problem relates to CVD layer/substrate compatibility and will be discussed later. The bottom of the layer appears indented in the section view due to chipping of the unsupported bottom surface during the cutting operation.

Since β-Si_3N_4 is the preferred phase in contact with molten silicon, an attempt was made to increase the β-phase content of the CVD oxynitride layers by high-temperature deposition. At temperatures above about 1200°C, gas-phase reaction led to the formation of amorphous powdery layers. At present, the fastest, most efficient, and least costly method of obtaining β-Si_3N_4 coatings by CVD is by depositing amorphous SiO_xN_y layers and subsequently heating the layers in contact with molten silicon. In silicon sessile drop experiments, this material, a few mil in thickness, has been held in contact with molten silicon at 1450°C in He for periods up to 40 h. During this period, the samples were thermally cycled about eight times to the test temperature and back to room temperature. Section micrographs of these samples show fractures in the layers caused by fracturing of the silicon droplet upon cooling. Otherwise the layers appear to maintain most of their original thickness. The full potential of these layers in contact with the silicon melt has not yet been determined.

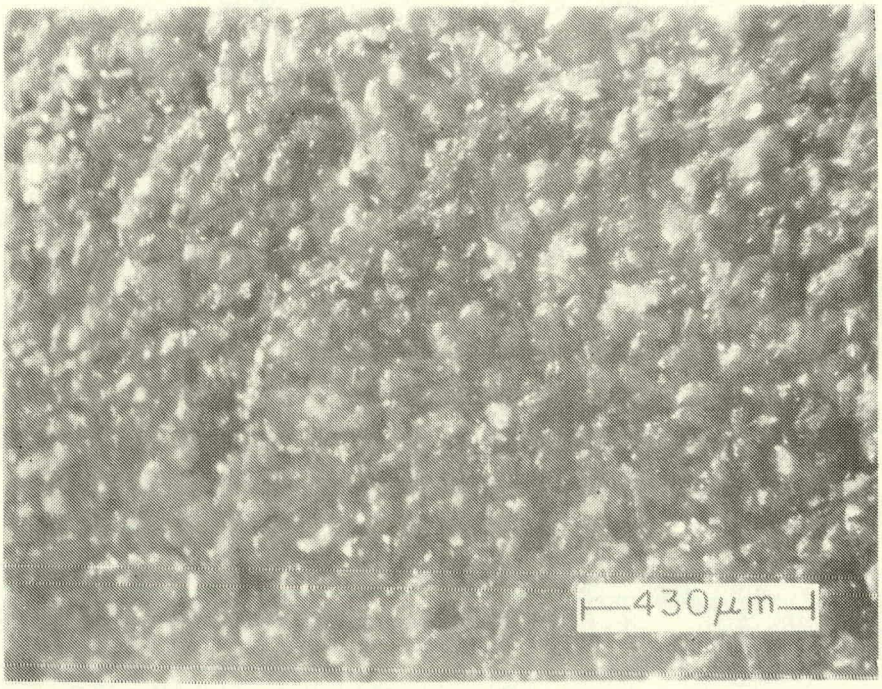

(a)

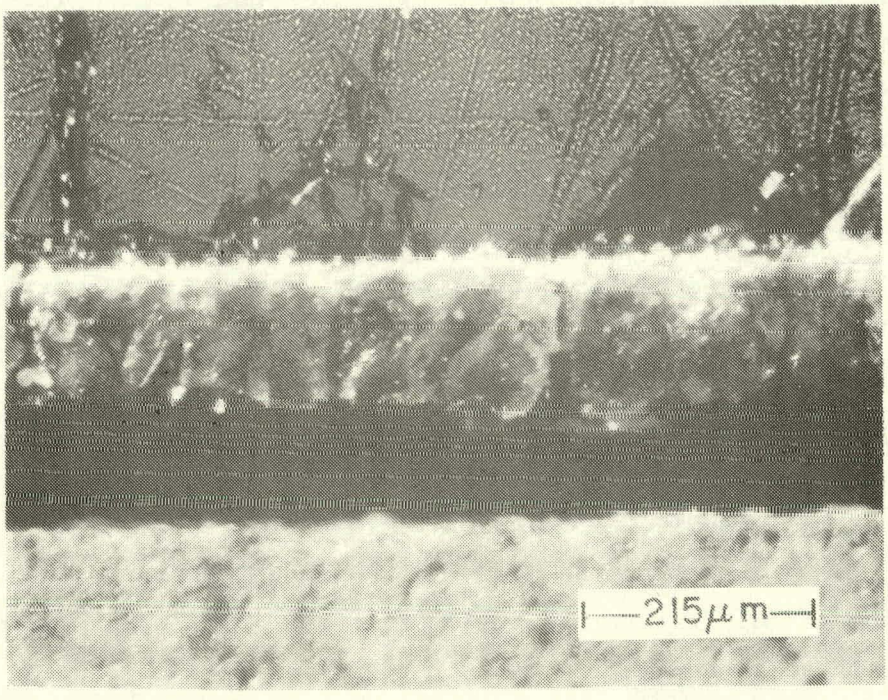

(b)

Figure 6. Surface topograph and section view of $Si/SiO_xN_y/RS\text{-}Si_3N_4$ composite after heating in He at 1450°C for 20 h.

D. REFRACTORY SUBSTRATE MATERIALS

The experiments described above indicate that β-Si_3N_4 has excellent chemical resistance to molten silicon. A major problem, however, in the development of this system is finding sufficently inexpensive substrate materials which are compatible with the system in terms of thermal expansion and purity. For example, the layer shown in Fig. 6 has separated from the substrate, although this may have occurred in the cooling-down process. Both vertical and horizontal cracks have been observed in CVD layers depending upon layer thickness and the nature of the substrate material. This enables molten silicon to penetrate into the layers and cause degradation by particulate erosion. An example is shown in Fig. 7 for the case of CVD Si_3N_4 ($\sim$1 mil) on graphite, where the duration of the heat treatment at 1440°C in He was about 30 min. Nevertheless, the extent of reaction is less than that for silicon on graphite, also shown in Fig. 7. The following materials were selected as the most suitable substrates for further testing: hot-pressed (HP) Si_3N_4, reaction-sintered (RS) Si_3N_4, sintered Si_2ON_2, vitreous carbon, mullite, and graphite.

The impurity content of these materials is usually very high, as shown in Table 6. Included in the table, also, is the impurity content of a CVD Si_3N_4 layer which was removed from a graphite susceptor used in coating these and other substrates, including BN. The contamination of this sample is probably a worst-case situation, yet the impurity level is well below the impurity levels for the various substrates coated. This is an example of the potential usefulness of CVD coatings as contact materials for molten silicon. The density of these commercially available materials may not exceed 75% of theoretical density, and considerable outgassing may occur at the silicon melt temperature. In the case of mullite, the elements Si, K, and Al were found by x-ray fluorescence in amorphous condensates on the water-cooled walls of the reaction vessel. The major difficulty in such cases is obtaining sufficient adherence between CVD layer and substrate at the silicon melt temperature. Some improvement in layer adherence, in the case of Si_3N_4 and Si_2ON_2 substrates, has been attained by preliminary heat treatment in N_2 or NH_3 at temperatures above the melting point of silicon.

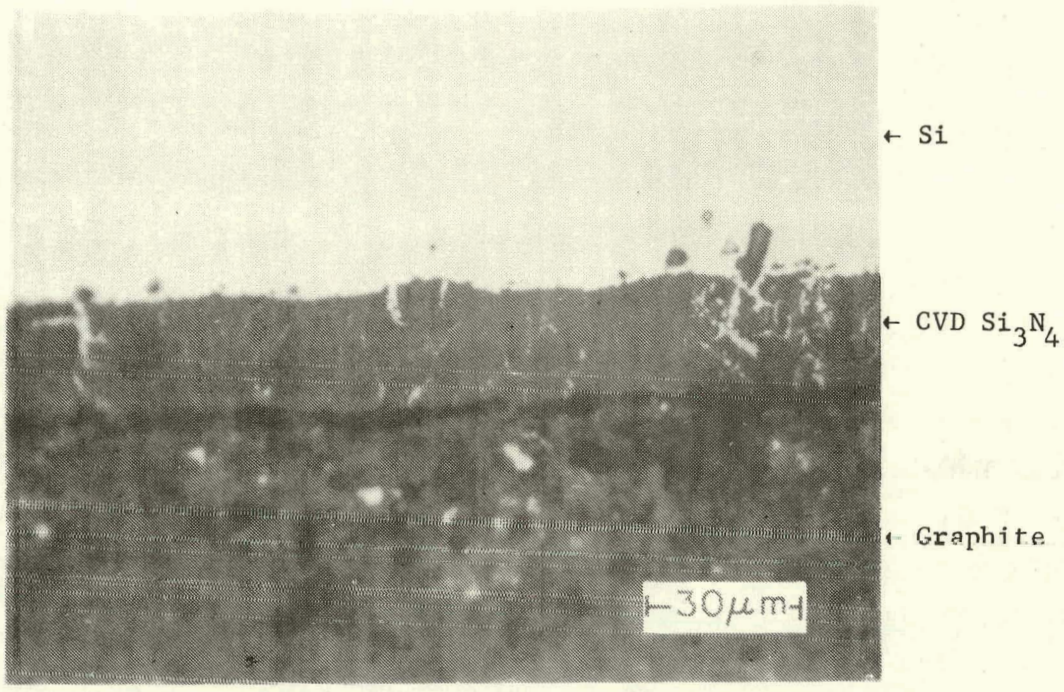

(a)

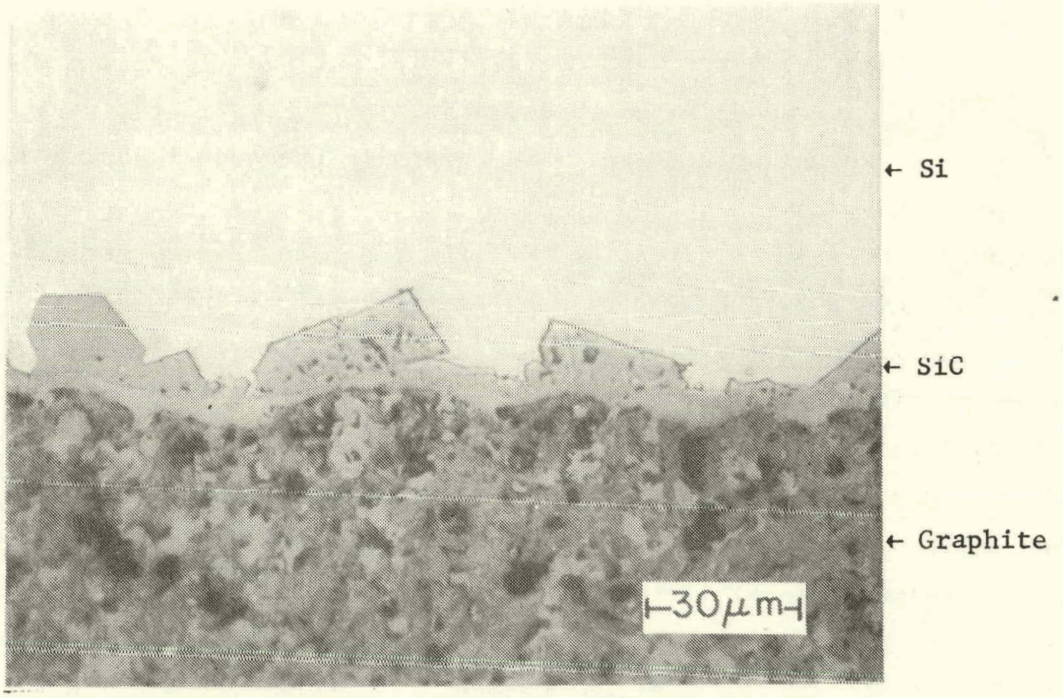

(b)

Figure 7. Section view of a Si/DFP-1 (graphite) sample; (a) with CVD Si_3N_4 coating, (b) without CVD coating.

TABLE 6. EMISSION SPECTROGRAPHIC ANALYSIS OF NITRIDE AND OXYNITRIDE (PPMW)

	Hot-Pressed Si_3N_4	Hot-Pressed Si_3N_4	Reaction-Sintered Si_3N_4	Sintered Si_2ON_2	CVD Film Si_3N_4
Cu	6-60	60-600	60-600	30-300	0.1-1
Ti	30-300	300-3000	300-3000	60-600	--
V	--	20-200	20-200	--	--
Ba	1-10	100-1000	10-100	10-100	--
B	15-150	60-600	6-60	30-300	10-100
Si	S	S	S	S	S
Mg	0.3%-3%	0.3%-3%	30-300	100-1000	1-10
Mn	1-10	100-1000	100-1000	150-1500	0.3-3
Cr	--	100-1000	60-600	60-600	--
Fe	30-3000	60-600	500-5000	600-6000	0.3-3
Al	0.6%-6%	1%-10%	1%-10%	600-6000	3-30
Be	--	3-30	0.6-6	--	--
Mo	--	3-30	30-300	20-200	--
Ca	30-300	600-6000	300-3000	600-6000	--
Ni	3-30	60-600	100-1000	10-100	--
Na	--	--	--	50-500	--
Co	--	--	--	6-60	--
Zr	--	--	--	6-60	--

In addition to the evolution of impurities, some of these materials are also subject to other changes at high temperature. Table 7 shows the approximately phase content of pressed and sintered Si_2ON_2 before and after immersion in molten silicon at 1440°C for 1 h in Ar. The data show that Si_2ON_2 is converted to α- and β-Si_3N_4 in the presence of molten silicon, and the rate of conversion of the surface region, in direct contact with the silicon melt, is more rapid than that of the subsurface region. This is similar to the case of CVD SiO_xN_y amorphous layers except that the ratio of β to α phase is greater in the latter case. However, the impurity content of Si_2ON_2 may influence the results. The trend is toward β-Si_3N_4 as the more stable phase in contact with the silicon melt. Changes have also been observed in the

TABLE 7. PHASES PRESENT IN Si_2ON_2 BOTH BEFORE AND AFTER IMMERSION IN MOLTEN SILICON

Sample Region	Treatment	Approximate Content Si_2ON_2	α-Si_3N_4	β-Si_3N_4
Bulk	As received	90%	5%	5%
Surface	After immersion in molten silicon for 1 h at ~1440°C in Ar	25%	30%	45%
Subsurface	After immersion as stated	70%	10%	20%

case of mullite. An example is shown in Fig. 8, which is a section view of a mullite crucible wall, which had been coated on the inner surface with CVD SiO_xN_y and used for melting silicon. The temperature was maintained a few degrees above the melting point for about 30 min. Microscopic examination, in addition to a scratch test, indicated that the wall of the crucible had been altered in mechanical properties in both the inner and outer surface regions. The central region of the wall retained its original hardness.

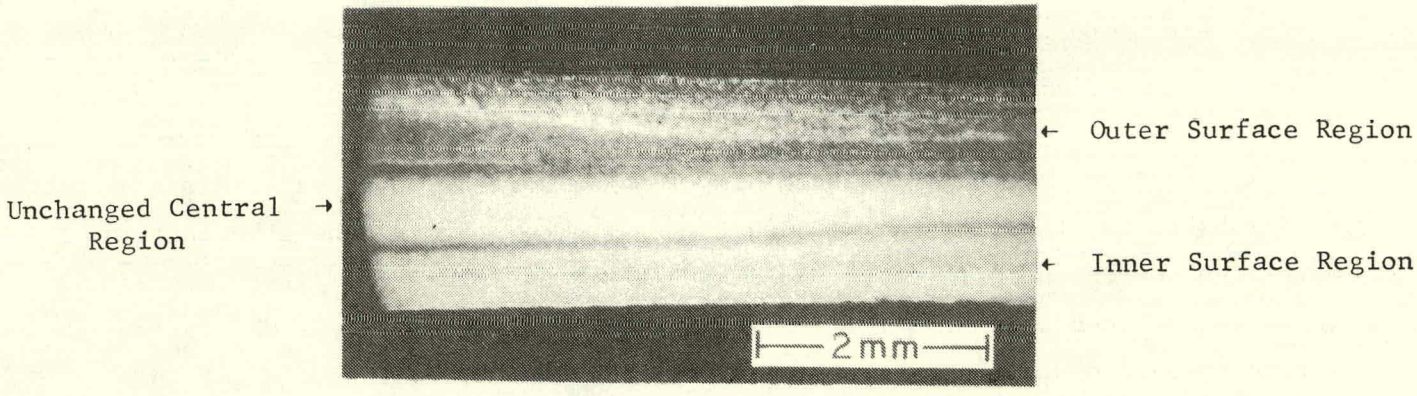

Figure 8. Section view of a mullite crucible wall which had been coated with silicon oxynitride on the inner surface and used for melting silicon (~30 min).

The best substrate results were obtained with high-density hot-pressed Si_3N_4 which was specially prepared for these experiments. The Si_3N_4 powder

was obtained from Cerac, Inc.*, as "Electronic Grade" with average particle size of 1-3 μm. Our analysis, by x-ray diffraction, indicated that the β-phase content was 75-80% and the α-phase content 20-25%. The densification aid was MgO "Baker-Analyzed" Reagent and was fired at 950°C for 1 h to remove water. The MgO content was 3.8% by weight and was mixed with the Si_3N_4 powder in CCl_4 using an ultrasonic homogenizer operating at 20 kHz. The CCl_4 was subsequently evaporated. Ball milling was avoided to reduce contamination. Hot-pressing took place in a floating graphite die containing a liner of carbon cloth which had been coated on the inside with BN. The graphite ram faces were similarly lined and coated. Hot-pressing was carried out at 1750°C for 1-1/4 h in N_2 at a pressure of 41.3 MN/m^2 (6000 psi). The density, compensated for the presence of MgO, was 99.2% of the theoretical value. The hot-pressed material was found to be β-phase Si_3N_4 by x-ray diffraction. Microscopic examination (550X) of a sectioned sample showed the presence of a small amount of a gray second phase, probably MgO from incomplete homogenization of the starting materials. The formation of a glassy MgO-SiO_2 phase between grains as reported by others[10] would not be detected at this magnification. Because of the chemical inertness of β-Si_3N_4 to molten silicon, a sample of this material, without a CVD coating, was used in a sessile drop experiment. A micrograph of a sectioned sample is shown in Fig. 9. The composite had been heated at 1450°C for 4 h in ultrapure helium. At the magnification used (~700X), the presence of a second phase in either the silicon droplet or on the Si_3N_4 surface was not detected. The roughness of the substrate surface appears to be about the same as observed before the sessile drop test. We have also noticed that the silicon droplet displayed little evidence of surface slag formation in contrast to previous experience with purchased hot-pressed Si_3N_4. These results provide further evidence for the inertness of β-Si_3N_4 to molten silicon. The resistivity of the silicon sessile drop was about 1 Ω-cm (n-type). The silicon was initially n-type with a resistivity of several hundred Ω-cm.

The results of emission spectroscopic analysis on the impurity content of the component materials both before and after this test are given in Table 8. It is interesting to note that some of the impurities present in the Si_3N_4 powder source material and hot-pressed Si_3N_4 are below detection

*Cerac, Inc., P.O. Box 1178, Milwaukee, WI 53201

10. G. R. Terwilliger and F. F. Lange, J. Am. Ceram Soc. 57, 25 (1974).

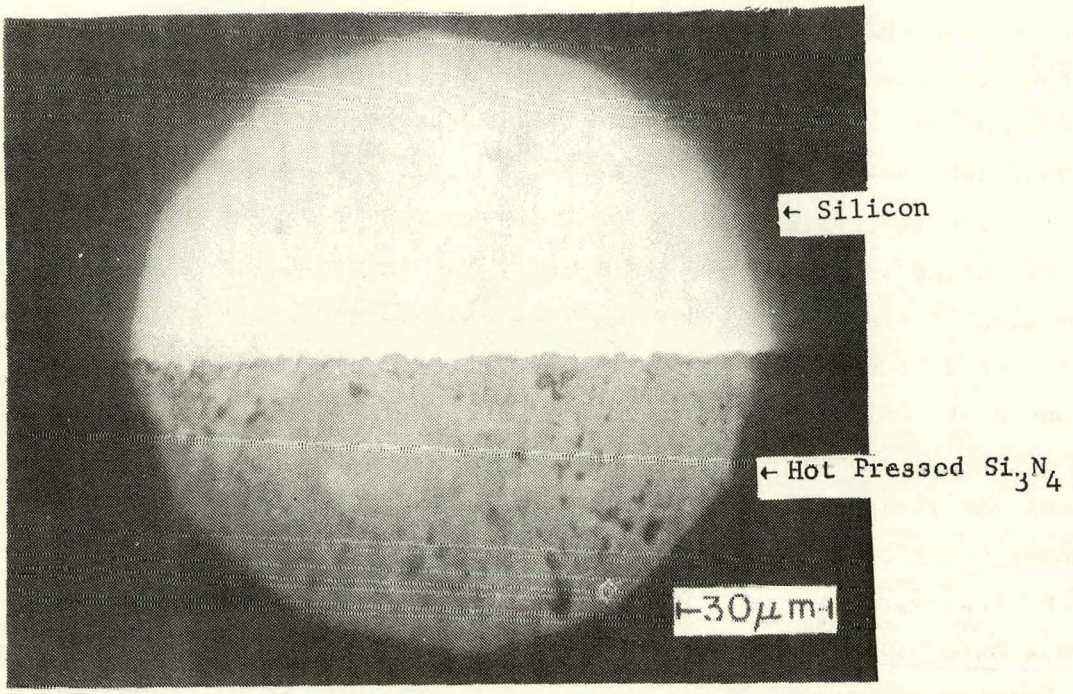

Figure 9. Section view of Si/Si_3N_4 (hot-pressed) sample after heating at 1450°C in He for 4 h.

TABLE 8. IMPURITY CONTENT (PPM) OF MATERIALS IN SILICON SESSILE DROP EXPERIMENT

Element	Si_3N_4 (Powder)	Si_3N_4 (Hot-Pressed)	Si (Sessile Drop)	Si (Source)
Al	600-6000	600-6000	30-300	3-30
Ba	10-100	10-100		
B	30-300	100-1000	60-600	50-500
Ca	30-300	30-300		3-30
Cu	5-50	6-60	3-30	
Fe	10-100	15-150	10-100	0.6-6
Mg	15-150	(S)	3-30	1-10
Mn	5-50	10-100	1-10	10-100
Na	20-200			
Ni		3-30		
Sr		0.3-3		
Ti	10-100	20-200		3-30
Zr		1-10		

level in the silicon droplet. The aluminum content in the silicon is more than an order of magnitude lower in the silicon droplet than in the substrate. It should be noted also that, although MgO (to a level of 3.8% by weight) was used as binder in the hot-pressed substrate, the Mg content in the silicon droplet is low considering the amount of impurity available and the exposure time at the melt temperature. With the exception of Al and Fe, the impurity content of the sessile drop is not widely different from that of the silicon source. This is probably due to the relatively low reactivity of β-Si_3N_4 with molten silicon. In general, the data indicate that molten silicon can remain in contact with hot-pressed Si_3N_4 for a considerable length of time at 1450°C without acquiring the impurity content level of the substrate. Emission of impurities from this material at high temperature was not a problem, and further phase changes were not observed. The thickness of CVD layers that can be deposited on these substrates is limited mainly by thermal expansion mismatch. Obviously, the impurity levels indicated are far too high, but the results provide hope for the reduction of impurities in molten silicon when a CVD coating such as CVD Si_3N_4 or CVD SiO_xN_y is applied to the substrate surface.

E. SILICON RIBBON GROWTH AND CHARACTERIZATION

Silicon ribbon specimens were grown from coated V-shaped dies to test the viability of the CVD coatings and the electrical properties of the silicon. The die parts were principally vitreous carbon and graphite because of outgassing problems with most of the other materials described above. The high-density hot-pressed Si_3N_4 described above was not available for these experiments. The coating was usually CVD Si_3N_4 because of the order in which the coatings were developed. Vitreous carbon was used as substrate in the hottest part of the die (side pieces) and high-density graphite in the cooler parts (end pieces). This arrangement was determined by the possibility of silicon penetrating into cracks in the coating and causing warpage in the component parts. The silicon ribbon was typically 1 in. wide, 30 to 40 mil thick, and 5 to 10 cm long. The duration of the experiments at the melt temperature was usually about 4 h.

A section view of a capillary at the bottom of a die after a growth run is shown in Fig. 10. The main features of the ribbons were parallel grains extending along the <211> growth direction. The orientation of the silicon

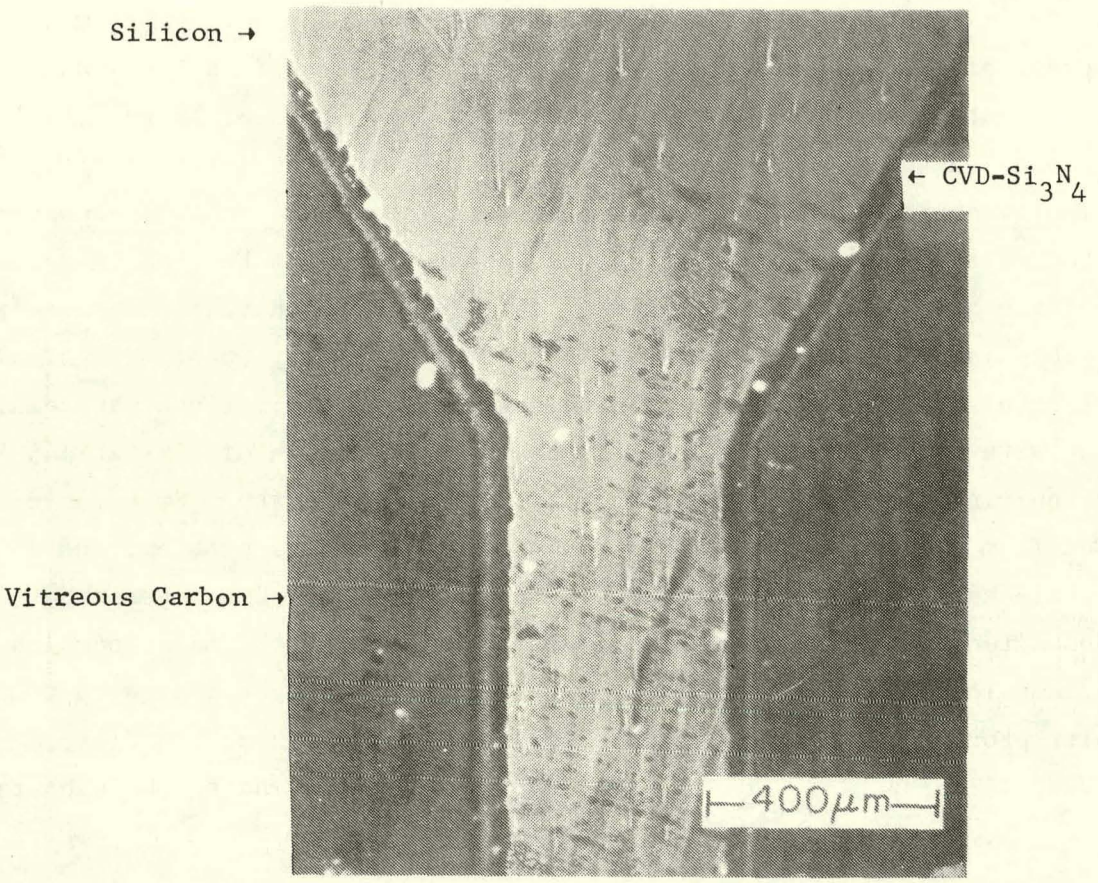

Figure 10. Section photograph of CVD-coated die after ribbon growth experiment.

seed was usually {110}<211>. Resistivity values up to 40 Ω-cm were obtained when peripheral materials such as thermal trimmers and graphite susceptors were fired at high temperature before die assembly. The spreading-resistance profile of a silicon ribbon across its width, which was about 2 cm, is shown in Fig. 11[11]. This ribbon had a uniform resistivity of 8-9 Ω-cm across its width. The central region of the ribbon was twinned single crystal, while the edges were polycrystalline. The dislocation density was $\sim 10^3/cm^2$ in the central region and increased to $\sim 10^6/cm^2$ at the edges.

Some ribbons were doped with boron to about 1 Ω-cm during growth for the fabrication of solar cells. Infrared transmission measurements were made on some samples to determine carbon and oxygen content relative to the Czochralski silicon seed. Oxygen and carbon were found in the latter at levels of about 35 ppma and 30-40 ppma, respectively, while these species were below detection

11. T. P. O'Donnell, Jet Propulsion Laboratory, California Institute of Technology, Pasadena, CA, private communication. (We gratefully acknowledge permission to present Figure 11 from the results of an independent evaluation by the Contract Monitor.)

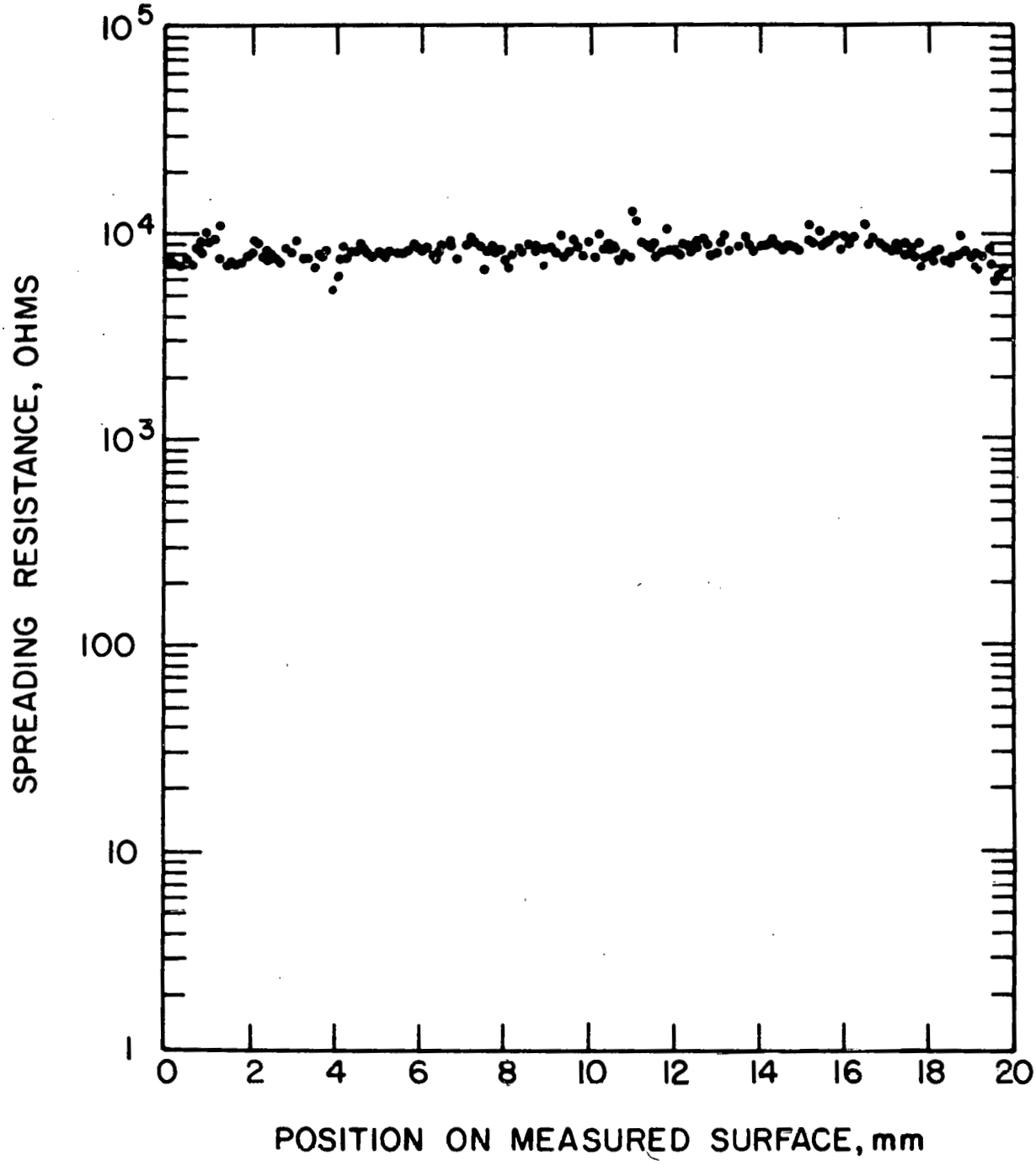

Figure 11. Results of spreading resistance measurements made across the width of a silicon ribbon which was grown from a CVD-coated die.

level for the technique employed in the silicon ribbons (<5 ppma for O and <25 ppma for C).

Solar cells were fabricated in a few ribbon specimens. For comparison, control cells were also fabricated simultaneously in Czochralski p-type silicon wafers of 1.5-Ω-cm resistivity. The fabrication was conducted by first etching the surfaces of the ribbon to remove ∿1 mil from each side followed by a standard $POCl_3$ junction formation diffusion at 875°C for 25 min. The samples were metallized with Ti/Ag on both sides, and a standard comb pattern was defined on the junction surface. The cells were delineated with a mesa etch to linear dimensions of 1.15 cm x 2.0 cm. No AR coating was applied before the first measurement. Cell illumination was provided by an ELH, AM-1 lamp simulator at 97 mW/cm^2. Estimates of the lifetimes (diffusion length) were obtained from pulsed recovery measurements on small mesa diodes adjacent to the cells.

Data obtained on two of the first ribbon specimens, pulled from a CVD Si_3N_4 coated die, are presented in Table 9. Two solar cells were fabricated on each ribbon specimen. The solar-cell characteristics for the control and ribbon samples, without antireflection (AR) coatings, are shown in Fig. 12-15. Results obtained on the ribbon specimen with the higher efficiency, after a single-layer AR coating (725 Å ZrO_2) was applied, are also given in Table 9. Cell performance comparable to the best cell in this Table was also obtained in subsequent measurements.

Portions of the two silicon ribbons (adjacent to the seed material) evaluated above were examined crystallographically. Results of the evaluation are presented in Appendix II. The analysis indicates that initial growth conditions are far from ideal. The formation of β-Si_3N_4 needles during simultaneous phase conversion and decomposition of CVD Si_3N_4 layers results in the incorporation of these needles into the ribbon material at the early stages for nucleation and growth. Despite this problem the results of the solar-cell evaluation are encouraging. It is clear from subsequent work that the application of CVD SiO_xN_y layers, which are more easily converted to β-Si_3N_4, would be superior in this application. Preferably, the conversion should be, at least, partially completed prior to using the die for ribbon growth. The changes occurring at the CVD layer surface are fastest during initial contact with molten silicon. One of the major difficulties, however, in the application of these layers is substrate compatibility, particularly thermal expansion properties and thermal and mechanical stability.

TABLE 9. RESULTS OF SOLAR-CELL MEASUREMENTS ON SILICON RIBBONS GROWN FROM COATED DIES

Property	Control Sample (No AR Coating)	Ribbon Specimen # 2-10-78			Ribbon Specimen # 2-1-78	
		Cell 1 (No AR Coating)	Cell 1 (With AR Coating)	Cell 2 (No AR Coating)	Cell 1 (No AR Coating)	Cell 2 (No AR Coating)
Lifetime, τ (μs)	3.6	0.9		0.9	0.6	0.6
Diffusion length ($L = \sqrt{D\tau}$) (μm)	95	48		48	39	39
Sheet resistance of junction layer ($\Omega/\square$)	48	48		49	57	60
J_{sc} (mA/cm^2)	21	18.5	27	18.3	16.6	17.4
V_{oc} (mV)	565	550	562	530	510	502
P_{max} (mW)	21.4	18		16.6	14.7	143
η (%)	9.6	8.0	11.8	7.4	6.6	6.4
FF	0.789	0.767	0.769	0.744	0.759	0.711

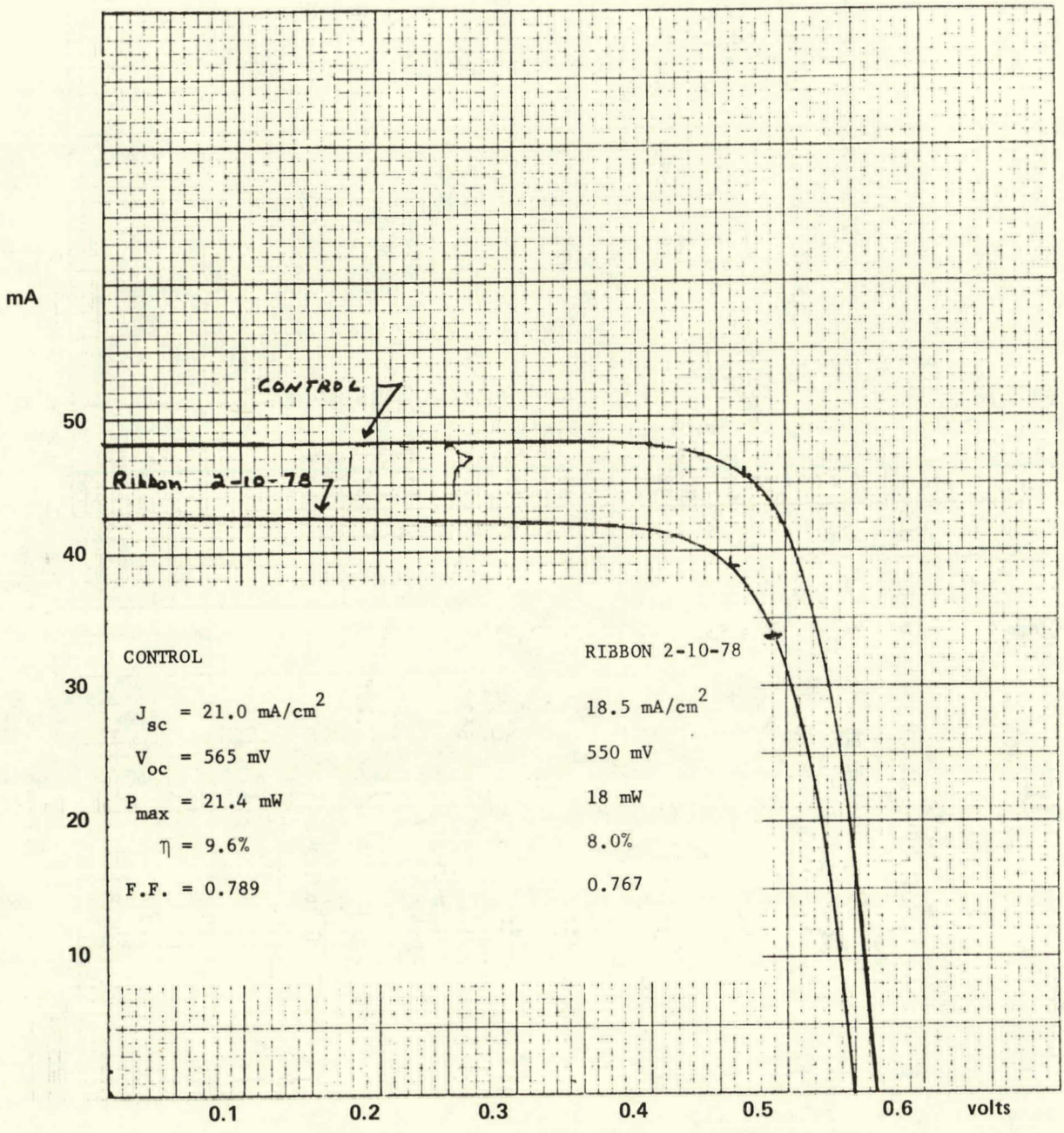

Figure 12. Solar-cell characteristics for one of two cells on ribbon 2-10-78 and for control cell without AR coatings.

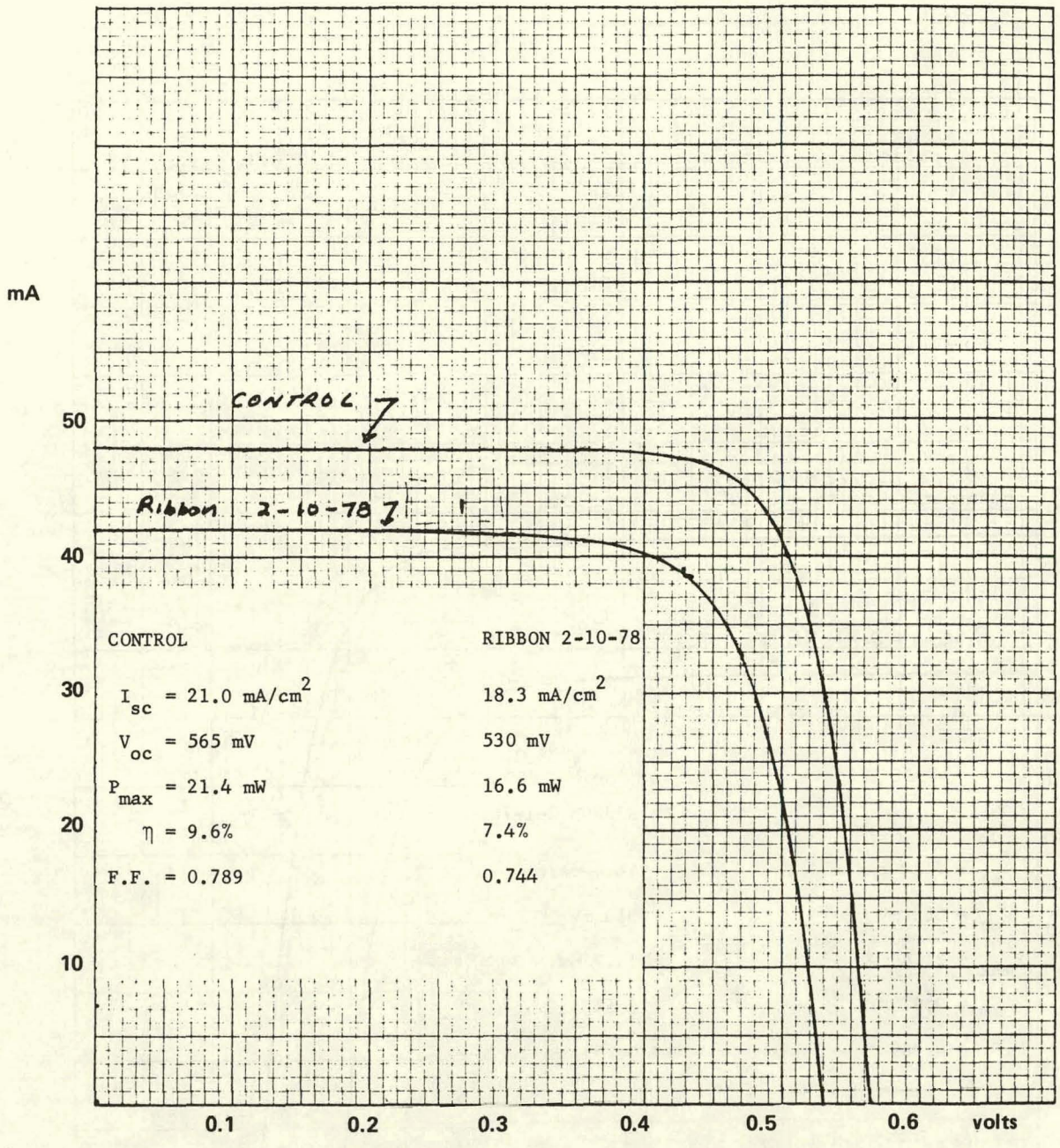

Figure 13. Solar-cell characteristics for second cell on ribbon 2-10-78 and for control cell without AR coatings.

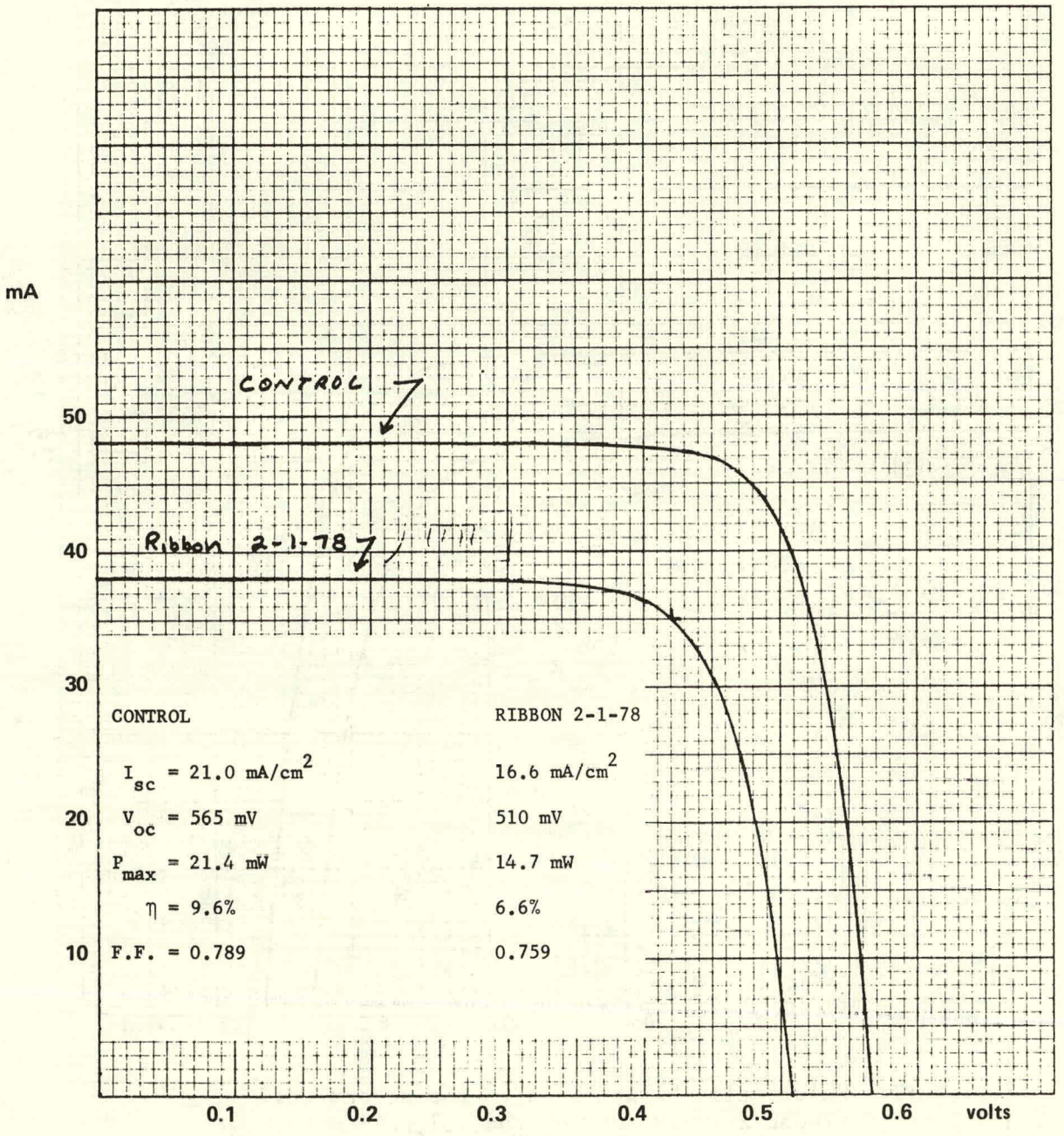

Figure 14. Solar-cell characteristics for one of two cells on ribbon 2-1-78 and for control cell without AR coatings.

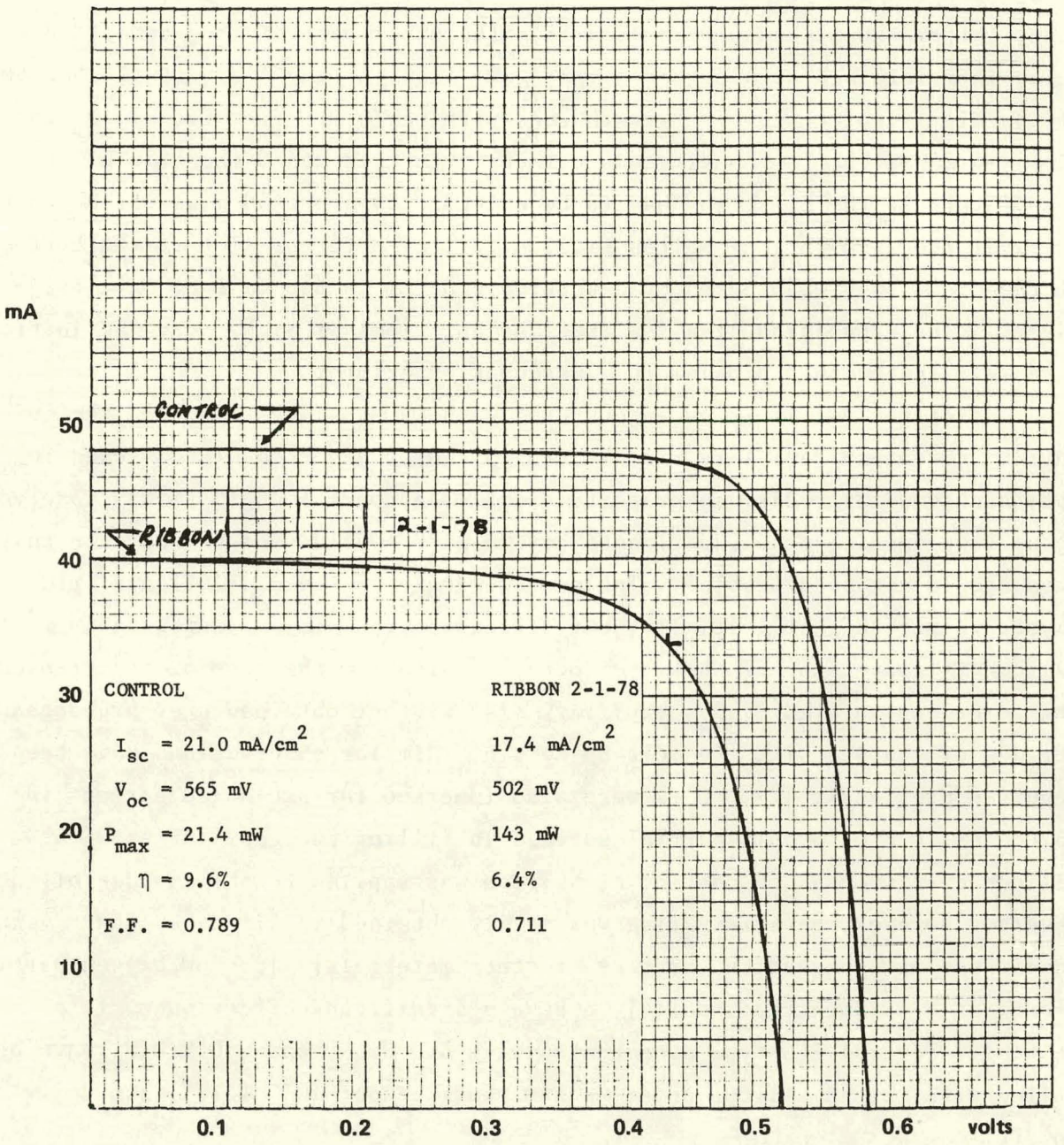

Figure 15. Solar-cell characteristics for second cell on ribbon 2-1-78 and for control cell without AR coatings.

Die coatings were also tested by making consecutive growth runs to test the effect of thermal cycling. Five consecutive runs were made from CVD Si_3N_4 dies (~2 mil Si_3N_4 on vitreous carbon). The nitride layer at this point (after ~20 h) had been eroded from the upper part of the V-shaped die which is maintained at a higher temperature than the capillary at the bottom of the die. Two consecutive growth runs were performed from CVD SiO_xN_y coated dies (~0.25-mil SiO_xN_y on vitreous carbon). In this case, the time at the melt temperature in the first run had to be extended by about 90 min, which was the interval required for the molten silicon to flow into the slot at the bottom of the die. This was caused by a wetting problem in the case of oxynitride layers. The deposition of a few thousand angstroms of Si_3N_4 over the initial layer eliminated this problem in subsequent experiments.

One of the difficulties encountered with CVD coatings has been the inability to obtain capillary rise in EFG-type dies under conditions used in obtaining capillary rise in graphite dies. The contact angle (~50°) observed in silicon sessile drop experiments on CVD Si_3N_4 would seem to indicate that this should not be a problem. The contact angle in the case of oxynitride layers is much higher initially, but decreases with time of exposure to molten silicon as conversion of the layer occurs. Also, in the case of hot-pressed and reaction-sintered Si_3N_4, capillary rise was not obtained over prolonged periods of contact with the melt up to 3 h. Similar observations have been reported previously[12]. Dies were also immersed for prolonged periods in molten silicon with only partial success in filling the capillaries with silicon even when a CVD coating of silicon was applied to the surface of the layers. However, capillary rise was easily obtained in all cases under vacuum conditions as reported in the case of other materials[13]. Low oxygen partial pressures have been reported[14] to have a significant effect on surface wetting. Several EFG-type dies coated with CVD Si_3N_4 and CVD SiO_xN_y have been filled with molten silicon under vacuum conditions (~10^{-2} Torr), and delivered to JPL.

---

12. G. H. Schwuttke, T. F. Ciszek, and A. Kran, "Silicon Ribbon Growth by a Capillary Action Shaping Technique," Final Report, DOE/JPL-954144-78/1.
13. R. R. Willis and D. E. Nietz, "Development and Evaluation of Refractory Dies and Containers," Eleventh Project Integration Meeting (Low-Cost Solar Array Project), Jet Propulsion Laboratory, California Institute of Technology, Pasadena, CA 91103, December 1978.
14. P. E. Grayson, L. A. Addington, P. D. Ownby, B. B. Yu, and M. W. Barsoum, "Study Program to Develop and Evaluate Die and Container Materials for the Growth of Silicon Ribbons," Quarterly Report No. 5 DOE/JPL-954877-78/3.

SECTION V

COST ANALYSIS FOR CVD COATING DIES AND CRUCIBLES WITH SILICON NITRIDE AND SILICON OXYNITRIDE

This estimate is based on the operation of standard RCA production barrel-type CVD reactor. Three alternative NH_3 - SiH_4 mixtures have been analyzed. The details are provided in the exhibit with the final cost in (¢/mil-in.^{2}). This allows costs to be estimated for dies with any thickness of coating or area. An example calculation is given in the exhibit for the I.S.T. dies described in a final report for NASA Contract No. 954465, dated June 1977.

EXHIBIT: COST ESTIMATE FOR DIE COATING

I. Investment

Barrel reactor

First Cost	$60K
Life	7 years
Cost of Capital	9%
Area	250 ft^2

Thruput: 150 in.^{2} x 2 mil/hr x 0.90 availability = 270 mil-in.^{2}/hr

$$\text{Annual cost} = \frac{\$60K}{5.033} = \$11{,}921,$$

where 5.033 is the present value of an annuity of $1 for seven years at 9% return.

Let α = fraction of time machine is utilized, averaged over a 24 hr/day, 345 day/year work schedule.

$$\text{Then the average hourly cost} = \frac{\$11{,}921}{(345)\ (24)\alpha}$$

$$= \frac{1.44}{\alpha}\ \$/\text{hr}$$

$$= 144/\alpha\ ¢/\text{hr}$$

Since the deposition rate is 270 mil-in.^{2}/hr, assuming full-barrel reactor load, we have

$$\text{Investment cost} = 144/\alpha\ ¢/\text{hr} \times \frac{1\ \text{hr}}{270\ \text{mil-in.}^2}$$

$$= 0.533/\alpha\ ¢/\text{mil-in.}^2$$

II. Labor

a) 1 hourly operator per four systems at $5/hr, 35% fringe benefit cost and 10% shift differential

$(= 1 + \frac{2 \times 0.10}{3})$ requires

$5/hr x 1.35 x 1.067 x 100 ¢/$ = 720 ¢/hr

To convert to mil-in.^{2}, we have

$$\text{Cost} = 720\ ¢/\text{hr} \times \frac{1\ \text{hr}}{270\ \text{mil-in.}^2} = 2.67\ ¢/\text{mil-in.}^2$$

b) 0.1 maint. man per system average at $5.10/hr

$$\text{Cost} = \$5.10 \times 1.35 \times 1.067 \times 100 \times \frac{1}{270\ \text{mil-in.}^2} \times 0.10\ \text{man/system}$$

$$= 0.27\ ¢/\text{mil-in.}^2$$

c) Supervisory labor: 0.1 supervisor per system average at $7.65/hr

$$\text{Cost} = \$7.65 \times 1.35 \times 1.067 \times 100 \times \frac{1}{270} \times 0.10$$

$$= 0.41\ ¢/\text{mil-in.}^2$$

III. Expenses

Three cases are presented, one for each major NH_3 alternative.

Cost in $/hr of Barrel Reactor Operation

Case	I	II	III
SiH_3	$14.90/hr	$14.90	$14.90
NH_3	27.00*	6.75**	2.25***
H_2	3.00	3.00	3.00
Power	0.98	0.98	0.98
Engineering	1.00	1.00	1.00
Susceptor	3.00	3.00	3.00
	$49.88	$29.63	$25.13

* 5 nines pure, NH_3:SiH_4 = 33:1

** 4 nines pure, NH_3:SiH_4 = 33:1

***4 nines pure, NH_3:SiH_4 = 10:1

The cost per mil-in.^{2} then becomes

Case I: $\$49.88 \times 100\ ¢/\$ \times \frac{1}{270} = 18.47\ ¢/\text{mil-in.}^2$

Case II: $\$29.63 \times 100\ ¢/\$ \times \frac{1}{270} = 10.97\ ¢/\text{mil-in.}^2$

Case III: $\$25.13 \times 100\ ¢/\$ \times \frac{1}{270} = 9.31\ ¢/\text{mil-in.}^2$

IV. Miscellaneous Overhead

The 250 ft^2 of floor space costs about \$25K to construct and lasts about 20 years. This corresponds to a 9% annuity factor of 9.128. Heat, light, and air conditioning cost about \$300/year for this area. Other additional overhead is assumed to be negligible.

Therefore,

$$\text{Misc. overhead cost} = \left(\frac{\$25{,}000}{9.128} + 300\right)/(345 \times 24 \times \alpha)$$

$$= \$0.367/\alpha\ \$/\text{hr}$$

$$= (\$0.367/\alpha)(100/270) = 0.136/\alpha\ ¢/\text{mil-in.}^2$$

V. Average Cost Per mil-in.^{2} of Deposition

Investment:	$0.533/\alpha$	¢/mil-in.^{2}	
Labor:			
Direct	2.67	¢/mil-in.^{2}	
Maint.	0.27	¢/mil-in.^{2}	
Supervisory	0.41	¢/mil-in.^{2}	
Miscellaneous Overhead:	$0.136/\alpha$	¢/mil-in.^{2}	
Expenses:	9.31-18.47	¢/mil-in.^{2}	
Total	$0.669/\alpha$ +	21.82	Case I
		14.32	Case II
		12.66	Case III

Sample calculation for the experimental "V"-shaped dies used for JPL Contract No. 954465.

Case I: $(0.67 + 21.82) \times 6 \times 5 = 675$ ¢/die

Case II: $(0.67 + 14.32) \times 6 \times 5 = 450$ ¢/die

Case III: $(0.67 + 12.66) \times 6 \times 5 = 400$ ¢/die

Since a die coating is assumed to last 24 hours, the hourly cost of die coating per IST puller is as follows:

Case I: 675 ¢/die $\times \frac{1}{24} = 28$ ¢/hr

Case II: 450 ¢/die $\times \frac{1}{24} = 19$ ¢/hr

Case III: 400 ¢/die $\times \frac{1}{24} = 17$ ¢/hr

Note: The add-on cost to produce CVD silicon oxynitride for case III is 0.45 ¢/mil-in.^{2}.

Hence, the total cost for CVD silicon oxynitride is $(0.669/\alpha + 12.66 + 0.45)$ ¢/mil-in.^{2} = 14.279 ¢/mil-in.^{2}

COST POTENTIAL ANALYSIS FOR CVD-COATING DIES AND CRUCIBLES WITH SILICON NITRIDE AND SILICON OXYNITRIDE

This cost estimate is similar to the previous analysis with two modifications. The following modifications have been made, assuming the availability of low-cost silane, from the Union Carbide Process, and an increase in the chemical efficiency of a barrel-type CVD reactor with recirculation of gases. The potential cost of silane was estimated by a scaling factor of a ratio of the projected cost of polysilicon from the Union Carbide Process to the current cost of polysilicon.

I. INVESTMENT

Barrel reactor

First Cost	\$60K
Life	7 years
Cost of Capital	9%
Area	250 ft^2

Thruput: 150 $in.^2$ x 2 mil/hr x 0.90 availability
= 270 mil-$in.^2$/hr

$$\text{Annual cost} = \frac{\$60K}{5.033} = \$11{,}921,$$

where 5.033 is the present value of an annuity of \$1 for seven years at 9% return.

Let α = fraction of time the machine is utilized, averaged over a 24 hr/day, 345 day/year work schedule.

$$\text{Then the average hourly cost} = \frac{\$11{,}921}{(345)\ (24)\alpha}$$

$$= \frac{1.44}{\alpha}\ \$/\text{hr}$$

$$= 1.44/\alpha\ ¢/\text{hr}$$

Since the deposition rate is 270 mil-$in.^2$/hr, assuming full-barrel reactor load, we have

$$\text{Investment cost} = 144/\alpha\ ¢/\text{hr} \times \frac{1\ \text{hr}}{270\ \text{mil-in.}^2}$$

$$= 0.533/\alpha\ ¢/\text{mil-in.}^2$$

II. LABOR

- One hourly operator per four systems at \$5/hr, 35% fringe benefit cost and 10% shift differential

$(= 1 + \frac{2 \times 0.10}{3})$ requires

\$5/hr x 1.35 x 1.067 x 100 ¢/\$ = 720 ¢/hr

To convert to mil-in.^{2}, we have

$$\text{Cost} = 720\ ¢/\text{hr} \times \frac{1\ \text{hr}}{270\ \text{mil-in.}^2} = 2.67\ ¢/\text{mil-in.}^2$$

- 0.1 maint. man per system average at \$5.10/hr

$$\text{Cost} = \$5.10 \times 1.35 \times 1.067 \times 100 \times \frac{1}{270\ \text{mil-in.}^2} \times 0.10\ \text{man/system}$$

$$= 0.27\ ¢/\text{mil-in.}^2$$

- Supervisory labor: 0.1 supervisor per system average at \$7.65/hr

$$\text{Cost} = 7.65 \times 1.35 \times 1.067 \times 100 \times \frac{1}{270} \times 0.10$$

$$= 0.41\ ¢/\text{mil-in.}^2$$

III. EXPENSES

SiH_4	\$0.30**
NH_3	0.80*
H_2	1.00*
Power	0.50
Engineering	0.30
Susceptor	0.50
	\$3.40

Cost in \$/hr of barrel reactor operation

The cost per mil-in.^{2} then becomes

$$3.40 \times 100\ ¢/\$ \times \frac{1}{270} = 1.259\ ¢/\text{mil-in.}^2$$

*Assumes 90% chemical efficiency due to recirculation of reactive gases by pumping.

**Reduced cost of SiH_4 from Union Carbide polysilicon plant at \$8 per kg. of silicon.

IV. MISCELLANEOUS OVERHEAD

The 250 ft^2 of floor space costs about \$25K to construct and lasts about 20 years. This corresponds to a 9% annuity factor of 9.128. Heat, light, and air conditioning cost about \$300/year for this area. Other additional overhead is assumed to be negligible.

Therefore,

$$\text{Misc. overhead cost} = \left(\frac{\$25{,}000}{9.128} + 300\right)/(345 \times 24 \times \alpha)$$

$$= \$0.367/\alpha \ \$/\text{hr}$$

$$= (\$0.367/\alpha)(100/270) = 0.136/\alpha \ ¢/\text{mil-in.}^2$$

V. AVERAGE COST PER mil-in.^2 of DEPOSITION

Investment:	$0.533/\alpha$	$¢/\text{mil-in.}^2$
Labor:		
Direct	0.80	$¢/\text{mil-in.}^2$
Maint.	0.13	$¢/\text{mil-in.}^2$
Supervisory	0.20	$¢/\text{mil-in.}^2$
Miscellaneous Overhead	$0.136/\alpha$	$¢/\text{mil-in.}^2$
Expenses:	1.259	$¢/\text{mil-in.}^2$
Total	$0.669/\alpha + 2.389$	

Add on cost for coating crucible 8-in.-diameter, 5 3/4 in. deep, with CVD silicon nitride.

Area to be coated $\frac{\Pi}{4}(8)^2 + \Pi 8\,(5.75) = 194.78 \text{ in.}^2$

Cost from the previous cost analysis (Cost Analysis for CVD Coating Dies and Crucibles with Silicon Nitride and Silicon Oxynitride), case 3, $\alpha = 1$; a 2-mil coating would be

(194.79 in.^2) (2 mil) $(13.329 ¢/\text{mil-in.}^2)$ $\left(\frac{1}{100} ¢/\$\right) = \$51.92$

Revised cost from the previous cost analysis (Cost Analysis for CVD Coating Dies and Crucibles with Silicon Nitride and Silicon Oxynitride). assuming 90% chemical efficiency due to recirculation of gases by pumping and reduced cost of SiH_4 from Union Carbide Polysilicon Plant.

(193.79 in.^2) (2 mil) $(3.058 ¢/\text{mil-in.}^2)$ $\left(\frac{1}{100} ¢/\$\right) = \$11.91$

SECTION VI

SUMMARY AND CONCLUSIONS

Evaluation of the reactivity of molten silicon with CVD Si_3N_4 and CVD SiO_xN_y layers indicates that these materials are considerably more resistant to chemical attack than many of the refractory carbides, nitrides, and oxides commercially available. Simultaneously, these layers provide a useful barrier to impurity diffusion from the substrate material into molten silicon.

Results of x-ray analysis on the thermal stability of the layers, both in the presence and absence of molten silicon, show that the amorphous layers are converted to α- and β-Si_3N_4 at high temperature. The rate of conversion is higher in the presence of molten silicon. Amorphous CVD Si_3N_4 is converted initially to α-Si_3N_4 with a low β-Si_3N_4 content. The α phase is then slowly converted to the β phase accompanied by simultaneous decomposition. By contrast, amorphous CVD SiO_xN_y layers are converted predominantly to β- Si_3N_4 with a low α-Si_3N_4 content. In this process, oxygen is evolved, and there is no evidence for the existence of a Si_2ON_2 crystalline phase in the resulting layers. The analysis also indicates that β-Si_3N_4 is much more resistant to chemical attack by molten silicon than α-Si_3N_4. Consequently, CVD SiO_xN_y provides a useful means of obtaining relatively pure and inert β-Si_3N_4 as a substrate coating for prolonged exposure to molten silicon, while CVD Si_3N_4 layers are useful for shorter exposure times. The phase changes occurring in CVD SiO_xN_y layers have been observed also in the case of pressed and sintered Si_2ON_2.

Coated dies were tested in silicon ribbon growth experiments. The tests indicate that the dies can be reused in consecutive growth runs without serious degradation of the coatings due to thermal cycling. However, there is a thickness limitation on the CVD coatings, depending upon the substrate material used, which limits the total exposure time in contact with the silicon melt. Substrate compatibility was a limiting factor in this study.

The resistivity of silicon ribbon specimens grown from CVD-coated dies ranged up to 40 Ω-cm. A solar-cell efficiency of 11.8% (AM-1) was obtained on ribbon grown in a preliminary evaluation of coated dies. The carbon and oxygen content in the silicon ribbons was below that found in Czochralski silicon. There is difficulty in obtaining capillary rise in CVD-coated dies at atmospheric pressure in inert gas. However, this can be readily accomplished under vacuum conditions in the preparation of the dies.

REFERENCES

1. T. O'Donnell, M. Leipold, and M. Hagan, "Compatibility Studies of Various Refractory Materials in Contact with Molten Silicon," DOE/JPL-1012-77/6, March 1978.
2. M. H. Leipold, T. P. O'Donnell, and M. A. Hagan, J. Cryst. Growth, to be published.
3. K. M. Kim, S. Berkman, M. T. Duffy, A. E. Bell, H. E. Temple, and G. W. Cullen, Final Report, prepared for Jet Propulsion Laboratory, California Institute of Technology, Pasadena, CA, DOE/JPL-954465-77/2, June 1977.
4. G. W. Cullen, J. F. Corboy, and R. T. Smith, J. Cryst. Growth 31, 274 (1975).
5. G. W. Cullen, Heteroepitaxial Semiconductors for Electronic Devices, (Springer-Verlag, New York, 1978), p. 60.
6. S. Berkman, V. S. Ban, and N. Goldsmith, Heteroepitaxial Semiconductors for Electronic Devices, (Springer-Verlag, New York, 1978), p. 264.
7. H. J. Stein and H. A. R. Wegener, J. Electrochem. Soc. 124, 908 (1977).
8. M. E. Washburn, Ceramic Bulletin 46, 667 (1967).
9. K. H. Jack, J. Mater. Sci. 11, 1135 (1976).
10. G. R. Terwilliger and F. F. Lange, J. Am. Ceram. Soc. 57, 25 (1974).
11. T. P. O'Donnell, Jet Propulsion Laboratory, California Institute of Technology, Pasadena, CA 91103, private communication.
12. G. H. Schwuttke, T. F. Ciszek, and A. Kran, "Silicon Ribbon Growth by a Capillary Action Shaping Technique," Final Report, DOE/JPL-954144-78/1.
13. R. R. Willis and D. E. Nietz, "Development and Evaluation of Refractory Dies and Containers," Eleventh Project Integration Meeting (Low-Cost Solar Array Project), Jet Propulsion Laboratory, California Institute of Technology, Pasadena, CA 91103, December 1978.
14. P. E. Grayson, L. A. Addington, P. D. Ownby, B. B. Yu, and M. W. Barsoum, "Study Program to Develop and Evaluate Die and Container Materials for the Growth of Silicon Ribbons," Quarterly Report No. 5, DOE/JPL-954877-78/3.
15. F. Schmid, C. P. Khattak, T. G. Diggs, and L. Kaufman, J. Electrochem. Soc., 126, 935 (1979).

APPENDIX I

SECTION MICROGRAPHS FROM SESSILE DROP TESTS REFERRED TO IN TABLE 1

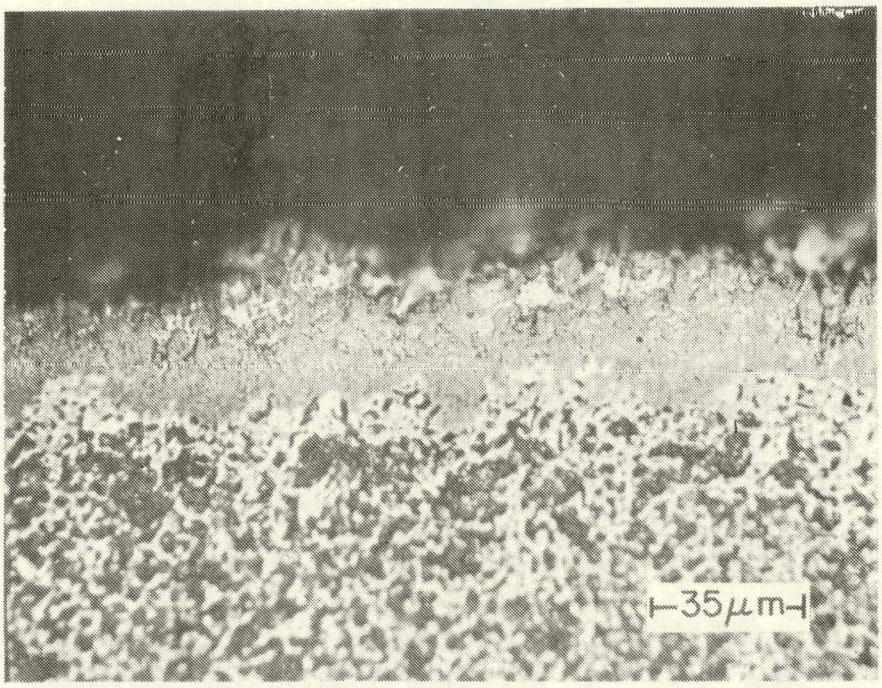

TiC

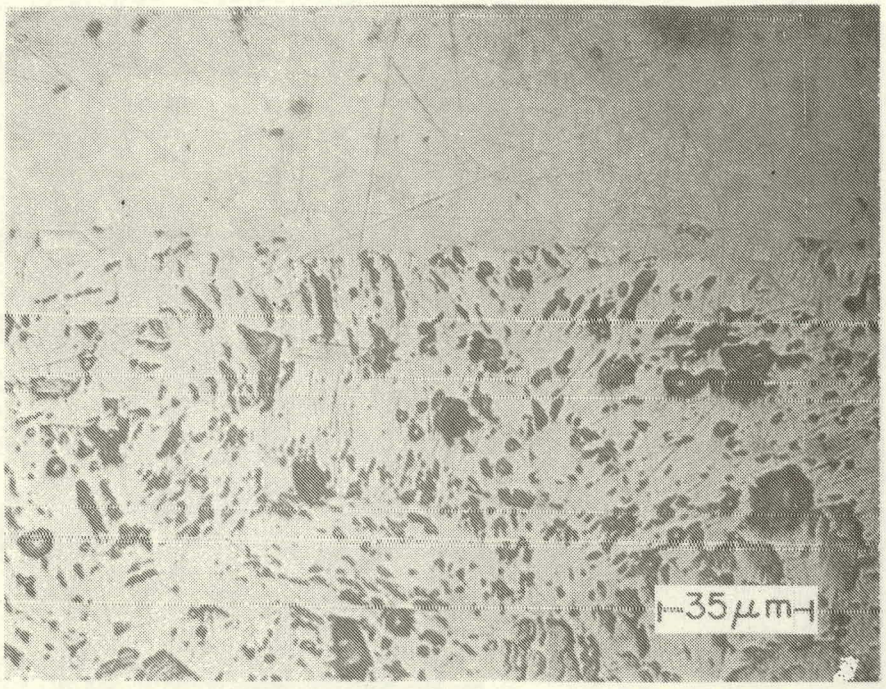

TiN

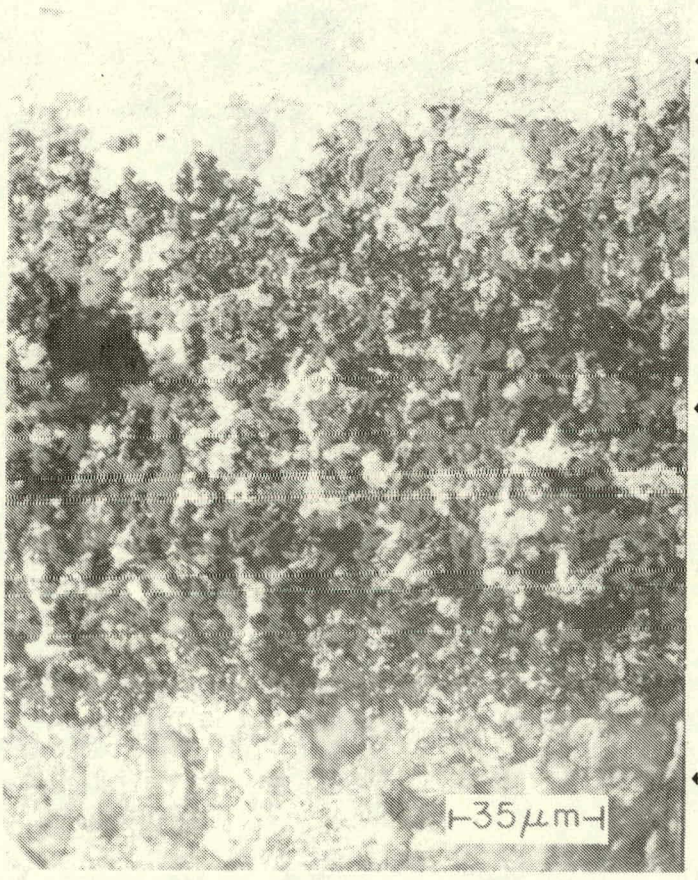
← Silicon
← Reaction Zone
← ZrN
⊢35μm⊣

ZrN

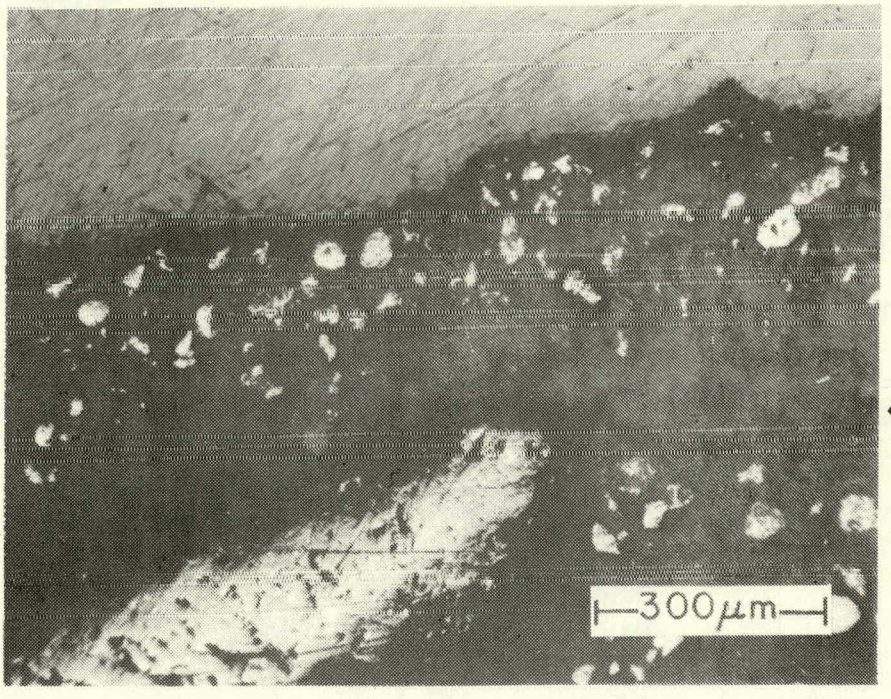
← Silicon
← AlN
⊢300μm⊣
Silicon in → AlN

AlN

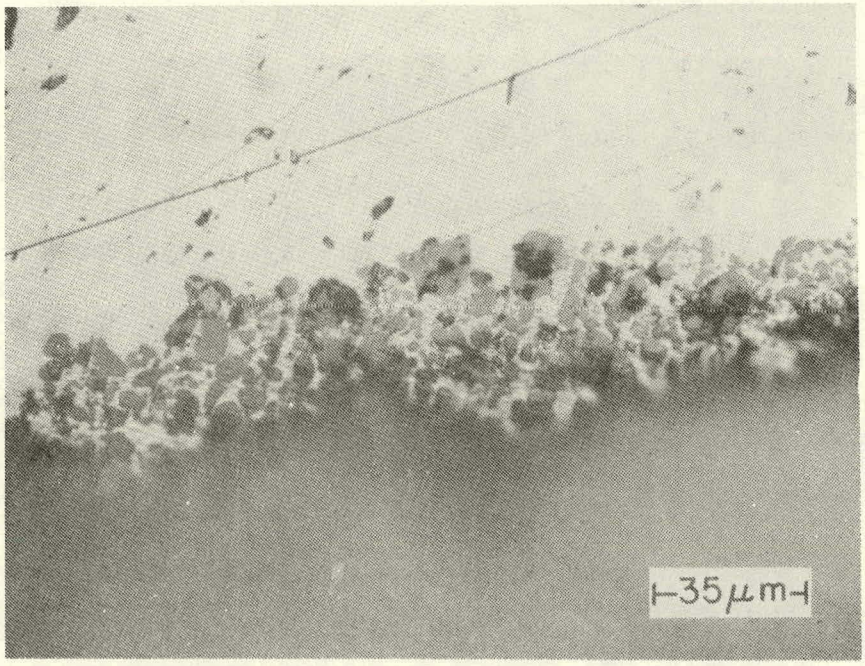

AlN + 5% SiC

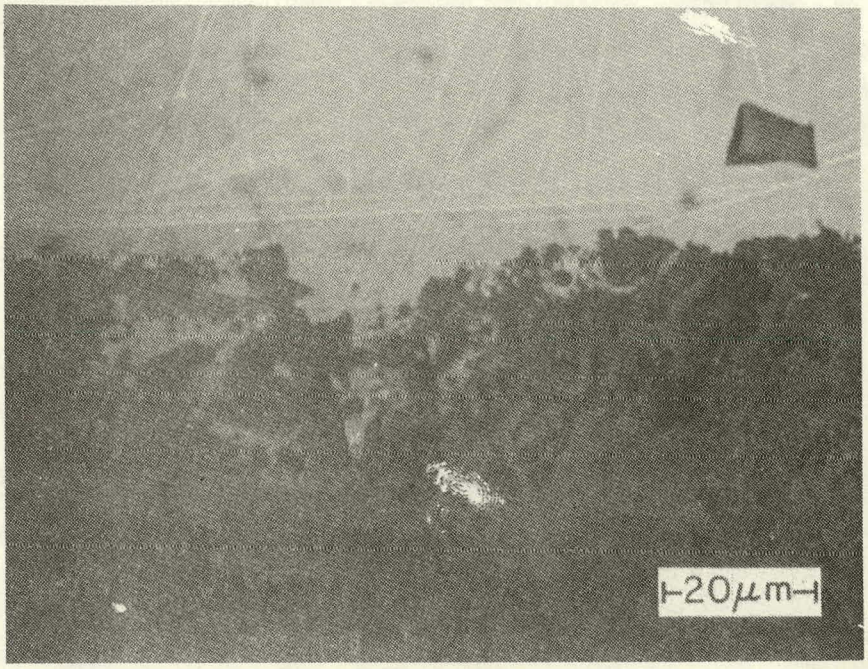

RS Si_3N_4

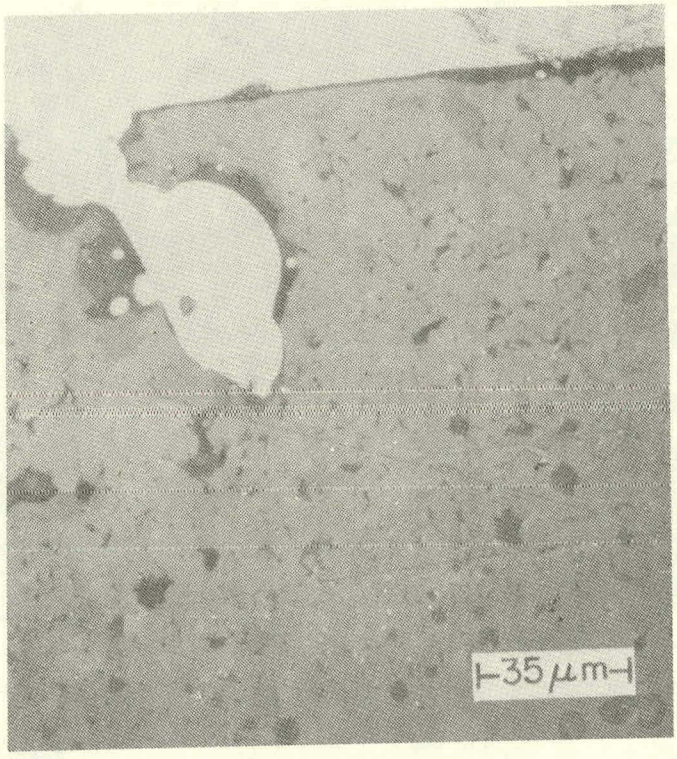

ZrO_2

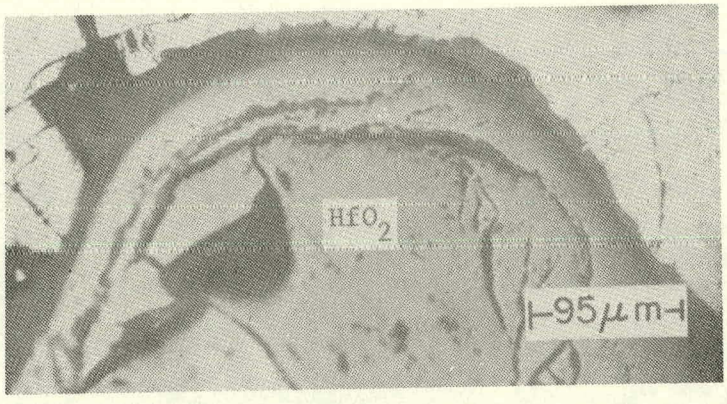

HfO_2

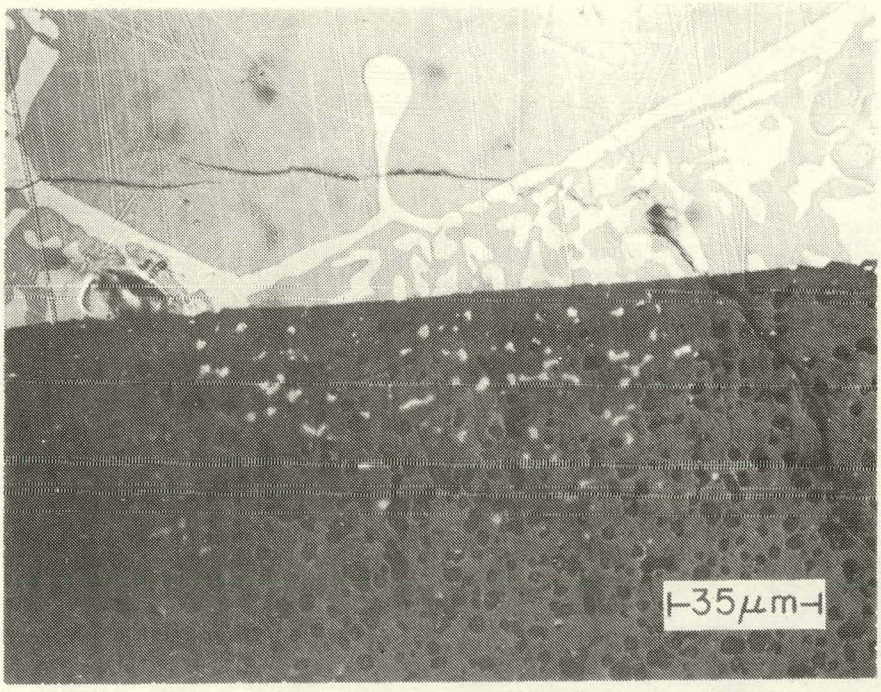

ThO_2

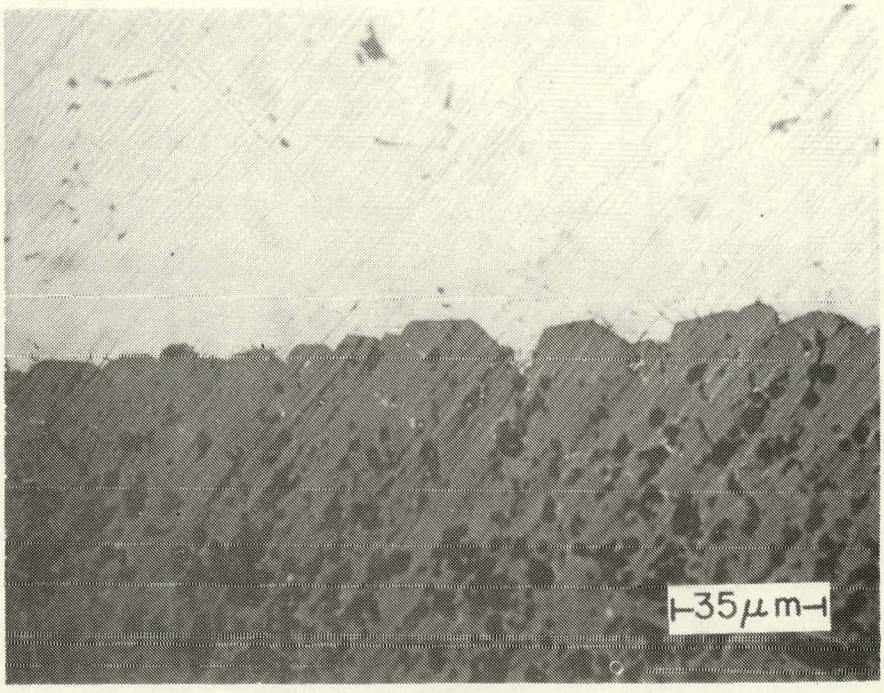

LaB_6

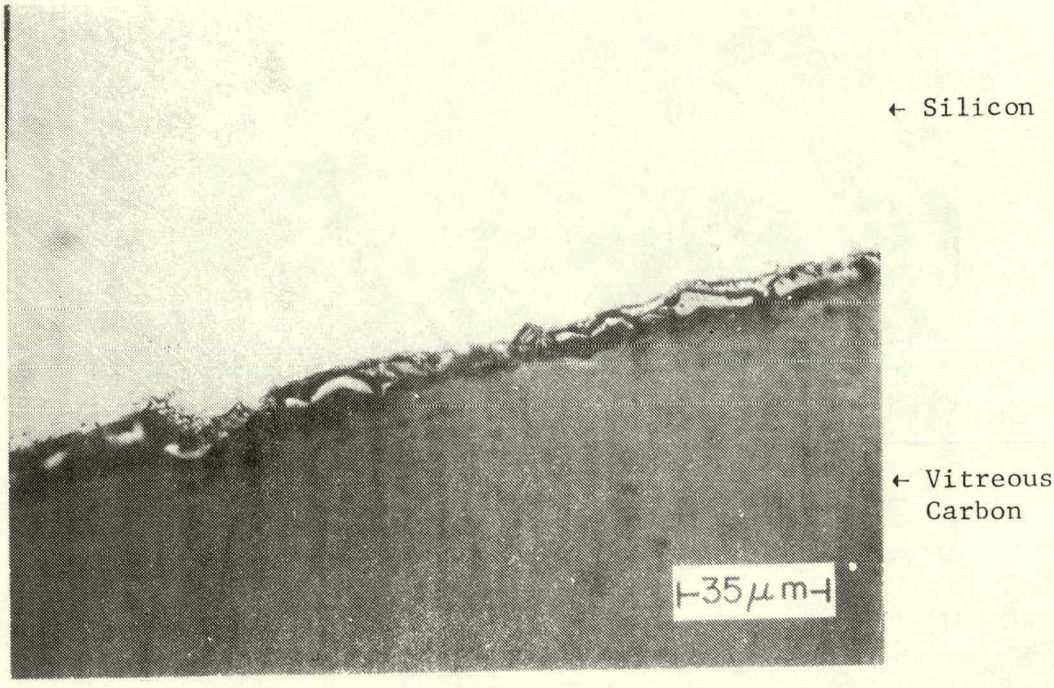

Vitreous Carbon

APPENDIX II

CRYSTALLOGRAPHIC EVALUATION OF SILICON RIBBON

APPENDIX II

The crystalline structure of two silicon ribbons, #2-10-78 and #2-1-78, grown from CVD-Si_3N_4/vitreous carbon composite dies, was characterized by x-ray topography and Sirtl etching. Previous solar-cell measurements (see Table 9 of this report) indicated that ribbon #2-10-78 had a higher cell efficiency than ribbon #2-1-78. In the two ribbons (β-doped, ∿1 ohm-cm), the oxygen and carbon concentration, measured by infrared absorption, were <5 ppma and <25 ppma, respectively.

Figures 1(a) and (b) are the $(\bar{1}11)$ x-ray projection topographs of #2-10-78 and #2-1-78, respectively. The ribbon surface is (110) and the growth direction is $[\bar{1}12]$ vertically upward in the topographs. The (111) diffracting plane is parallel to the growth direction and perpendicular to the ribbon surface. The major features of the two ribbons are a series of parallel grains shown as dark lines in Figs. 1(a) and 1(b), and multiple twinning which is revealed after Sirtl etching as seen in Figs. 2(a) and 2(b); the multiple twins are not imaged in the (111) topograph, since the twin plane is also the diffracting plane in this case. The misorientation of the grains should be mostly small, i.e., within ∿0.1°, since the Bragg condition for diffraction is met and the topographs show contrast. However, the ribbon section near the left edge of #2-1-78, for instance, has grains with large misorientation, so that the Bragg condition is not met and no contrast is observed [see Figure 1(b)]. Note that in the ribbon #2-1-78 a high level of strain is observed in several ribbon segments, which is obviously associated with the freeze-over of the ribbon during growth and the concurrent inclusion of particulates in the ribbon.

Figures 3(a) and (b) are the x-ray section and projection topographs of #2-10-78; $(\bar{2}20)$ is the diffracting plane which is perpendicular to the ribbon surface and lies at 55° to the ribbon-growth direction. The crystalline structure imaged in the $(\bar{2}20)$ projection topograph is about the same as observed previously in the $(\bar{1}11)$ topograph [see Fig. 1(a)]. In the section topograph, however, a number of grains with strain at the grain boundaries are imaged.

Multiple twinning has always been present in all silicon ribbons grown by the inverted Stepanov process using a BN die, in the inverted ribbon growth using CVD-Si_3N_4 composite dies, and the EFG process using graphite dies. In general, silicon is markedly susceptible to twinning during crystal growth.

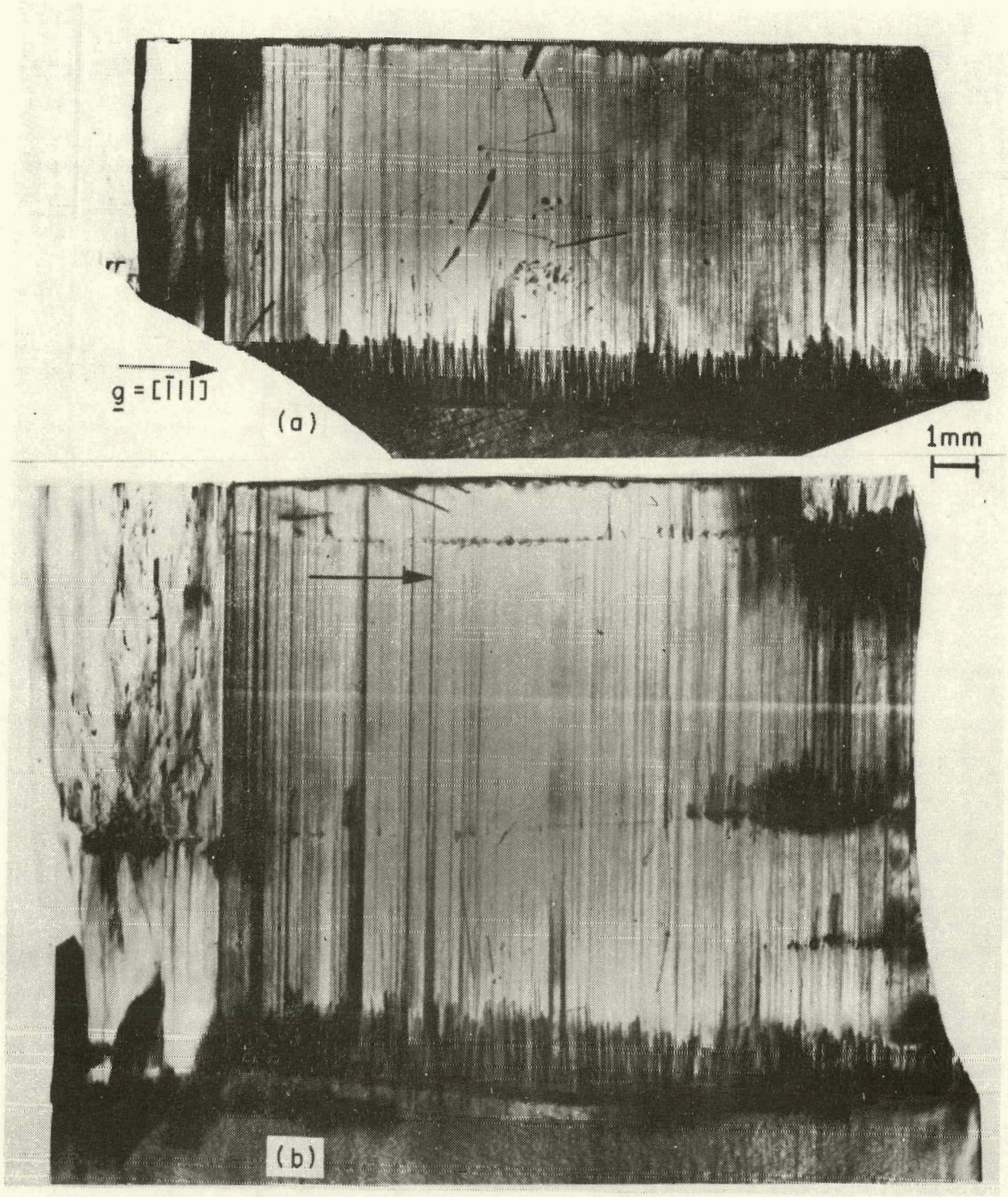

Figure 1. ($\bar{1}11$) x-ray projection topograph of (a) the silicon ribbon #2-10-78, and (b) #2-1-78. MoKα radiation.

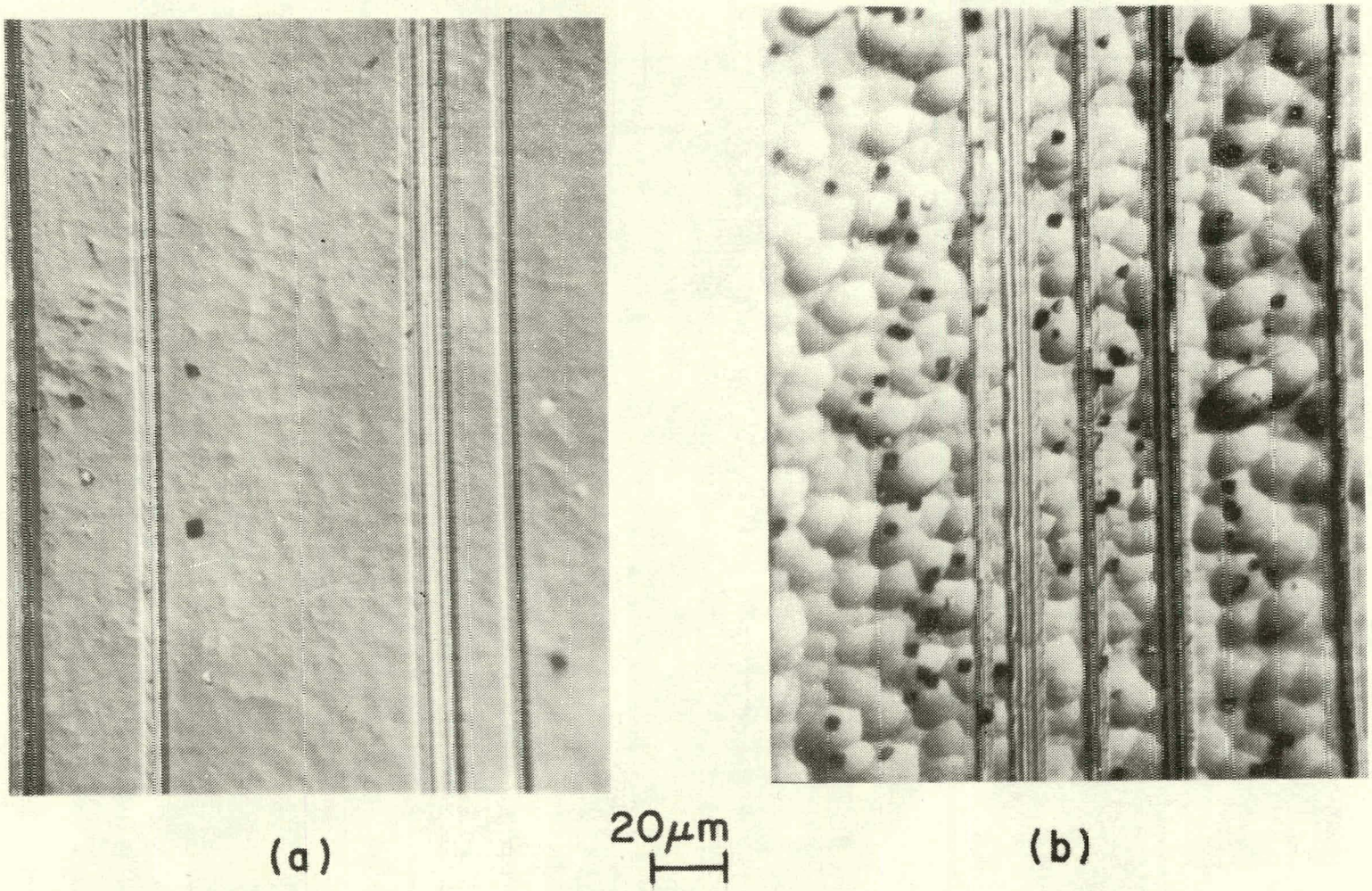

Figure 2. Optical micrograph after Sirtl etching, (a) #2-10-78, and (b) #2-1-78. Ncte the multiple twins and dislocation etch pits.

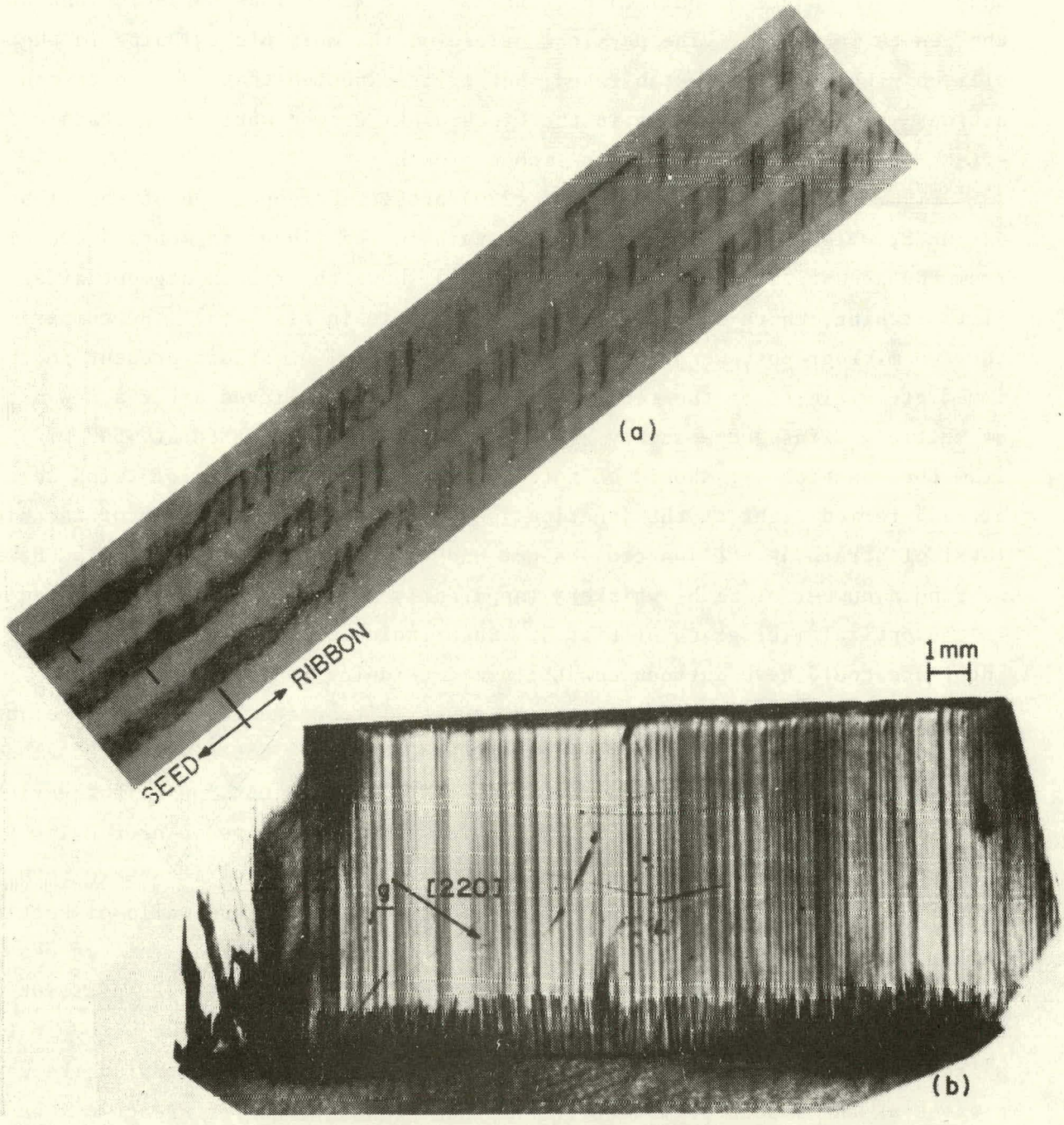

Figure 3. (a) $(\bar{2}20)$ x-ray section topograph, (b) $(\bar{2}20)$ projection topograph of #2-10-78. Note the grains and the associated strain in (a).

In Czochralski silicon-crystal growth, for instance, twinning occurs readily under sudden change of pull rate or temperature as well as by inclusions at the growth interface. The physical origin of the multiple twinning in the silicon ribbons is not established, but it is expected that the growth conditions which cause twinning in the Czochralski growth would be certainly effective in causing twinning in ribbon growth.

Figure 4(a) is a detail of the (220) projection topograph of the ribbon #2-10-78, which shows a high level of stain in the ribbon segments, ~600 μm from the seed-ribbon junction. Figure 4(b) shows the ribbon segment after Sirtl etching, which is indicated by a rectangle in Fig. 4(a). By comparing the two micrographs, we observe that the high level of strain present in the immediate vicinity of the seed-ribbon junction was relieved after a new set of multiple twins and possibly also new grains were generated at ~600 μm from the junction; it should be noted, however, that a number of twins were already formed right at the junction [see Fig. 4(b)]. The origin of the high level of strain at the junction is not understood at the present time. However, we find a number of Si_3N_4 whiskers (apparently β-Si_3N_4) at the junction as seen in the optical micrograph of Fig. 5. Such inclusions at the solid-liquid growth interface could have introduced strain and twinning in the ribbon.

It should be noted that the Si_3N_4 crystallites occurred only at the junction between the seed and the silicon ribbon, and were not distributed along the ribbon. Likewise, silicon carbide inclusions were not found in the ribbons, thus, indicating that the CVD Si_3N_4 coatings were effective in protecting the vitreous carbon walls of the dies. Silicon carbide crystallites have been identified, however, within the solidified silicon along the walls of sectioned dies. This may be due, in part, to the penetration of silicon into cracks in the coating followed by dissolution of carbon and subsequent precipitation of silicon carbide. In some cases, silicon carbide crystallites occurred in the silicon melt even when the die parts did not contain carbon but graphite was present as the susceptor material. In these cases, transport reactions were probably responsible for the formation of silicon carbide [15]. In all cases,

15. F. Schmid, C. P. Khattak, T. G. Diggs, and L. Kaufman, J. Electrochem. Soc., 126, 935 (1979).

the amount of silicon carbide precipitate present was small in comparison to the amount observed in uncoated vitreous carbon dies, and the crystallites were not dispersed through the silicon melt.

In summary, multiple twinning and a number of grains have been found in silicon ribbons #2-10-78 and #2-1-78. Such defect structure has been commonly observed in silicon ribbons grown by the inverted Stepanov, as well as EFG process. In ribbon #2-10-78, where a solar-cell efficiency of 11.8% was measured, we find a relatively low level of strain compared to the ribbon #2-1-78, where a lower efficiency was measured.

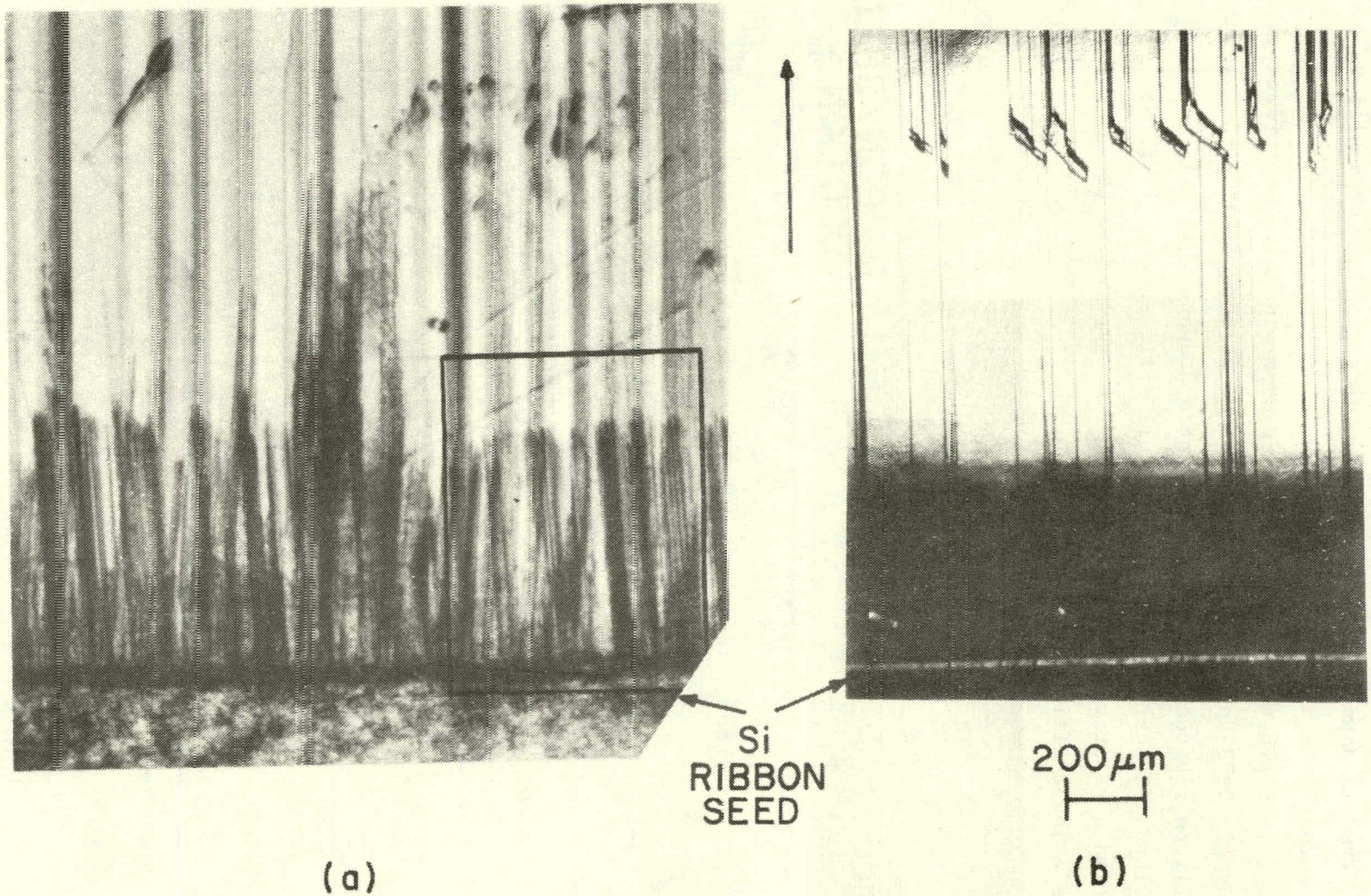

Figure 4. (a) Detail of $(\bar{2}20)$ x-ray projection topograph of #2-10-78, (b) optical micrograph of #2-10-78 after Sirtl etching of a ribbon segment rectangled in (a). Note that strain present within ~600 μm from the seed-ribbon junction is relieved by generation of a new set of twins and possibly alsc new grains.

Figure 5. Optical micrograph of the silicon ribbon at the seed-ribbon junction. Note the Si_3N_4 whiskers (apparently β-Si_3N_4) at the junction.

☆ U.S. GOVERNMENT PRINTING OFFICE: 1980-640-258/2210